DESIGN AND ANALYSIS OF MULTIPHASE DC-DC CONVERTERS WITH COUPLED INDUCTORS

A Thesis

by

MENG SHI

Submitted to the Office of Graduate Studies of
Texas A&M University
in partial fulfillment of the requirements for the degree of

MASTER OF SCIENCE

May 2007

Major Subject: Electrical Engineering

DESIGN AND ANALYSIS OF MULTIPHASE DC-DC CONVERTERS WITH COUPLED INDUCTORS

A Thesis

by

MENG SHI

Submitted to the Office of Graduate Studies of
Texas A&M University
in partial fulfillment of the requirements for the degree of

MASTER OF SCIENCE

Approved by:

Chair of Committee,	Prasad Enjeti
Committee Members,	Chanan Singh
	Sunil Khatri
	Sing-Hoi Sze
Head of Department,	Costas N. Georghiades

May 2007

Major Subject: Electrical Engineering

ABSTRACT

Design and Analysis of Multiphase DC-DC Converters with Coupled Inductors.

(May 2007)

Meng Shi, B.Eng., Shanghai Jiao Tong University, China

Chair of Advisory Committee: Dr. Prasad Enjeti

In this thesis, coupled inductors have been applied to multiphase DC-DC converters. Detailed analysis has been done to investigate the benefits of directly coupled inductors and inversely coupled inductors, compared to conventional uncoupled inductors. In general, coupled inductors for multiphase DC-DC converters have inherent benefits such as excellent current sharing characteristics, immunity to component tolerance and reduction in current control complexity. Specifically, by employing directly coupled inductors for multiphase DC-DC converters, overall current ripple can be effectively reduced, compared to that of uncoupled inductors. For inversely coupled inductors, phase current ripple can be reduced if operating points and coupling coefficients are carefully chosen. As for small-signal characteristics, inversely coupled inductors have the advantages of broadening the bandwidth of multiphase DC-DC converters and being more immune to load variation at low frequencies. On the other hand, directly coupled inductors have the benefit of low sensitivity to input variation at high frequencies. In addition, the proposed new structure for multiphase DC-DC converters has excellent current sharing performance and reduced current ripple. Computer simulations have been done and hardware prototypes have been built to validate the concepts.

DEDICATION

To my parents.

ACKNOWLEDGEMENTS

I am grateful to my academic advisor, Dr. Prasad Enjeti, for his guidance and encouragement throughout my graduate studies. Without his patience and continuous support, I could not have finished my graduate studies at A&M.

I would like to thank my committee members, Dr. Chanan Singh, Dr. Sunil Khatri, Dr. Sing-Hoi Sze, for their help, time and concern.

Also, I would like to thank all my fellow students working in the Power Electronics and Fuel Cell Power Conditioning Laboratory for their help and guidance.

TABLE OF CONTENTS

Page

CHAPTER Page

LIST OF FIGURES

Page

Page

Page

LIST OF TABLES

Page

CHAPTER I
INTRODUCTION

1.1 Introduction

During the past several decades, power electronics research has focused on the development of multiphase parallel DC-DC converters to increase the power processing capability and to improve the reliability of the power electronic system. The advantages of constructing a power converter by means of interleaved parallel connected converters are ripple cancellation in both the input and output waveforms to maximum extent, and lower value of ripple amplitude and high ripple frequency in the resulting input and output waveforms. In addition, multiphase parallel connection of power converters reduces maintenance, increases reliability and fault tolerance. In general, the interleaving technique consists of phase shifting the control signals of several converter cells in parallel, operating at the same switching frequency. Maximum benefits of interleaving can be achieved at certain operating point. Generally, for boost converter, a single-inductor, single-switch topology and its variations exhibit a satisfactory performance in the majority of applications where the output voltage is greater than the input voltage. Nevertheless, in a number of applications, such as power-factor correction circuits and distributed power conversion systems, the performance of the boost converter can be improved by implementing a boost converter with multiple switches and multiple boost inductors.

Although parallel individual DC-DC converters in interleaved structure have been

---

This thesis follows the style and format of *IEEE Transactions on Industry Applications.*

demonstrated to reduce the overall current ripple, it is still challenging to meet today's requirements. In addition, the multiphase interleaving structure has more inductors than the single phase converters, which increases the complexity of this converter.

Further, multiphase DC-DC converters operating in continuous inductor current mode have better utilization of power devices, lower conduction loss, and lower total current ripple. But in some cases it is also feasible to adopt the interleaved converter operating in discontinuous inductor current mode. For example, multiphase boost converters working in DICM have lower diode reverse-recovery loss and lower transistor switching-on loss. However, a major design problem among the parallel paths is current sharing. It can be shown that, when two similar but independently controlled DC-DC converters are connected in parallel, with the same input and output voltages, the converter with a larger duty cycle may operate in continuous inductor current mode, while the other will then automatically operate in discontinuous inductor current mode. Under this condition, any further additional loading current will be taken up by the converter in continuous inductor current operation. Thus, current sharing is very sensitive to the mismatch in duty cycle. The design of current-sharing control circuits has been discussed in some literature. A method of using hysteresis current control in a pair of boost converters with coupled inductors has also been suggested.

In addition, the overall current ripple reduction of conventional multiphase DC-DC converters has not been extended to inductors and switches. Large phase current ripples not only increase the conduction losses but also increase the turn-off losses of MOSFETs. The large current ripples in the inductors also increase the losses in the inductors. The current ripples in the MOSFETs and the inductors are the same as those in the converters

with the same number of channel in parallel. Although channel interleaving reduces the overall current ripple, it cannot reduce the current ripples in either the MOSFETs or the inductors. These ripples reduce steady-state efficiency. Also, in conventional multiphase DC-DC converters, current imbalance can occur due to the component tolerances or parameter variations. Therefore, those converters not only suffer from high ripple current on semiconductor devices, but also require individual phase currents sensed for current sharing purpose.

1.2 Conventional multiphase DC-DC converters with uncoupled inductors

Conventional multiphase interleaved boost converter with uncoupled inductors, as shown in Fig.1, are usually employed in high input-current and high input-to-output voltage conversion applications. As an example, an interleaved boost topology is sometimes used in high-power applications to eliminate reverse-recovery losses of the boost rectifier by operating the two boost converters at the boundary of continuous-conduction mode (CCM) and discontinuous-conduction mode (DCM) so that the boost switches are turned on when the current through the corresponding boost rectifier is zero. In addition, interleaving is also employed to reduce the input current ripple, as shown in Fig.2, and therefore to minimize the size of the input filter that would be relatively large if a single boost converter was used.

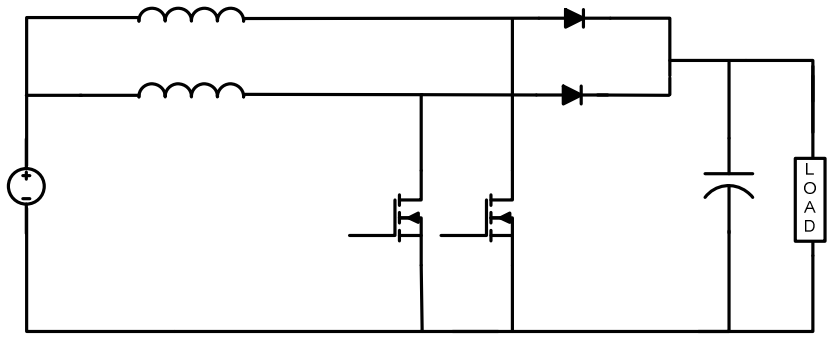

Fig. 1. Conventional multiphase interleaved boost converter.

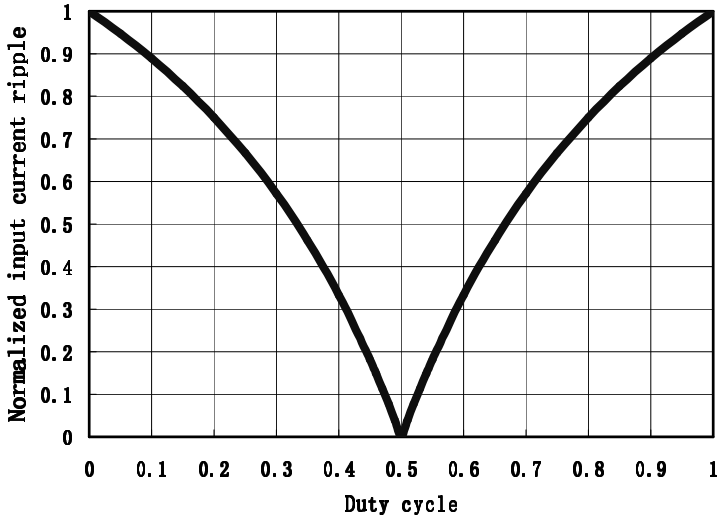

Fig. 2. Normalized overall current ripple versus duty cycle.

Similarly, traditional multiphase interleaved buck converters with individual inductors, as shown in Fig.3, greatly reduces the total current ripples flowing into the output capacitors. And since the output voltage ripple of a buck converter is mainly contributed by charging/discharging of the capacitor and ESR of the capacitor, which can be expressed as

$$\Delta Vo, c = \frac{\Delta Q}{C} = \frac{\Delta Ic}{8Cf}$$
$$\Delta Vo, esr = \Delta Ic \cdot ESR \tag{1}$$

Therefore, with the overall current ripple reduction by multiphase interleaved structure, the steady-state voltage ripples at the output capacitors are greatly reduced. This benefit yields smaller output inductances for the converter, for the same requirement for overall current ripple. Then the transient voltage spikes can also be reduced due to the smaller output inductances. A much smaller output capacitance can meet the requirements of both the transient voltage spikes and the steady-state output voltage ripples.

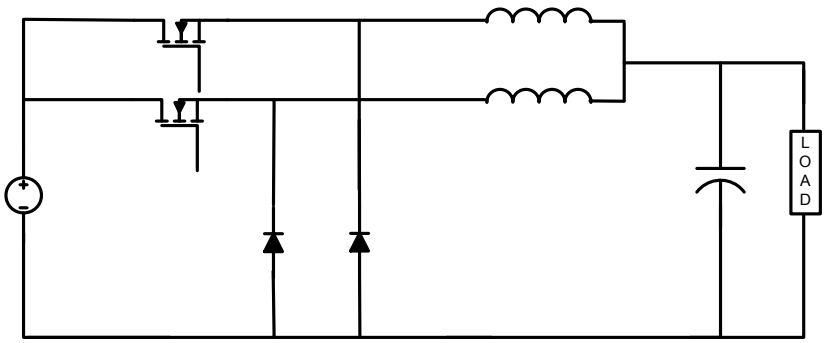

Fig. 3. Conventional multiphase interleaved buck converter.

1.3 Coupled inductor modeling

A coupled inductor is a device primarily used for energy storage during a power converter switching cycle, and the power entering the coupled-inductor is not the same as the power leaving it in a given instant. Transformers are used for voltage and current scaling, for dc isolation, and to obtain multiple outputs from a single converter. Coupled-

inductors are used to reduce converter volume by using one core instead of two or more, to improve regulation of power converters.

The equivalent circuit model of a two-winding coupled inductors is shown in Fig.4.

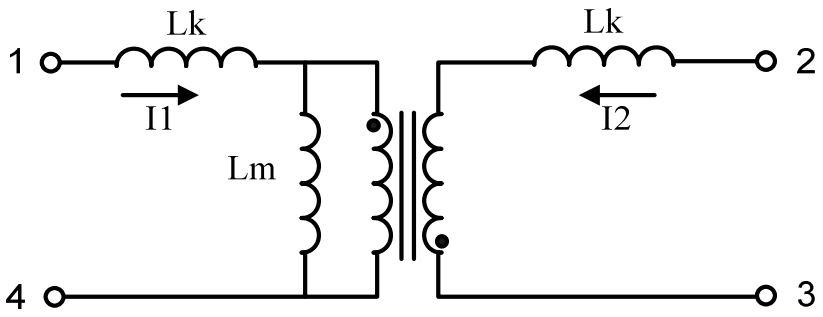

Fig. 4. Equivalent circuit model of coupled inductor.

To relate reluctance to the circuit elements depends on how the circuit elements are measured, and how this measurement equates back to the reluctance model. The first and most obvious measurement to take on the inductor component is to measure the open circuit inductance on each of the two windings. Fig.5 makes it clear that the measured open-circuit inductance equals

$$L_{open(1-4)} = L_{open(2-3)} = L_m + L_k \tag{2}$$

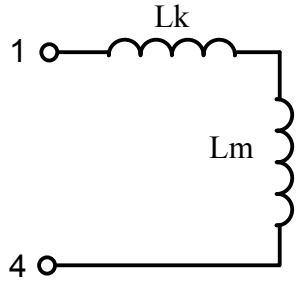

Fig. 5. Open circuit inductance.

In regards to the reluctance model, as shown in Fig.6, the open circuit inductance measurement on only one winding is equivalent to removing or opening the other source such that the equivalent circuit reduces to that shown in Fig.7.

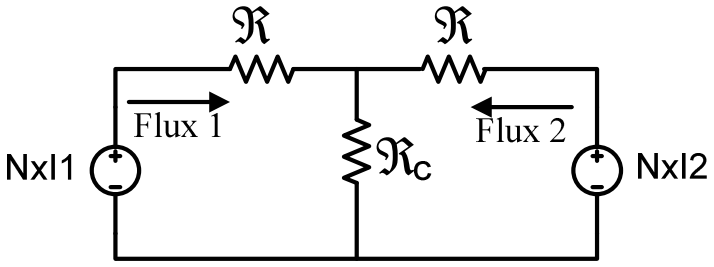

Fig. 6. Reluctance model of coupled inductor.

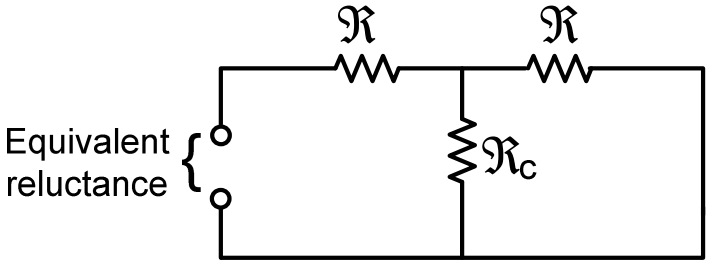

Fig. 7. Equivalent reluctance.

It is clear from this figure that the equivalent reluctance is equal to

$$\Re_{open(1-4)} = \Re_{open(2-3)} = \Re + (\Re_c \,||\, \Re) = \frac{2\Re\Re_c + \Re^2}{\Re_c + \Re} \tag{3}$$

Knowing that $L=N^2/R$, and using (2) and (3) yields

$$L_{open(1-4)} = L_{open(2-3)} = L_m + L_k = N^2 \frac{\Re_c + \Re}{2\Re\Re_c + \Re^2} \tag{4}$$

The second measurement on the inductor component could be to measure the short circuit inductance by measuring the inductance on one winding with the other winding shorted. Assuming a perfect short, the short-circuit inductance equals

$$L_{short(1-4)}(with\ 2\text{-}3\ shorted) = L_k + (L_m \| L_k) \tag{5}$$

If Lm>>Lk, then

$$L_{short(1-4)} = 2L_k \tag{6}$$

This is measurement is often used to measure the leakage inductance in transformer applications because it is assumed that Lm>>Lk. However, for the coupled inductor, this is not the case, and as such L_{short} does not lead to a clear or direct measurement of the leakage inductance. A better measurement is the reverse-series inductance, in which the windings of the inductor are tied in series but out of phase, as shown in Fig.8. In this measurement, the opposing polarity of winding effectively cancels the magnetizing inductance Lm and the series inductance equals

$$L_{reverse(1-2)}(with\ 3\text{-}4\ shorted) = 2L_k \tag{7}$$

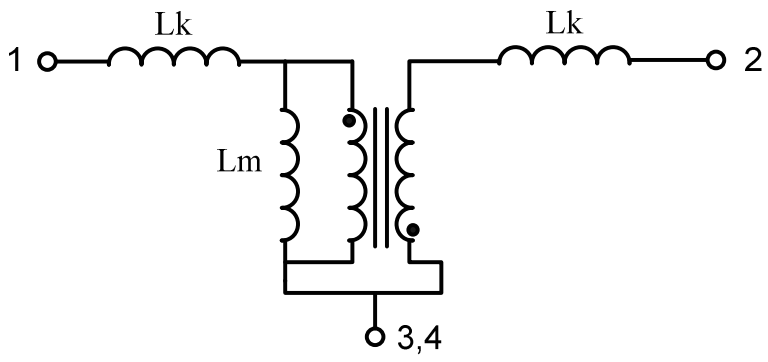

Fig. 8. Reverse series inductance.

In regards to the reluctance model, the reverse-series measurement is equivalent to putting the two windings in parallel, and the equivalent circuit reduces to that shown in Fig.9.

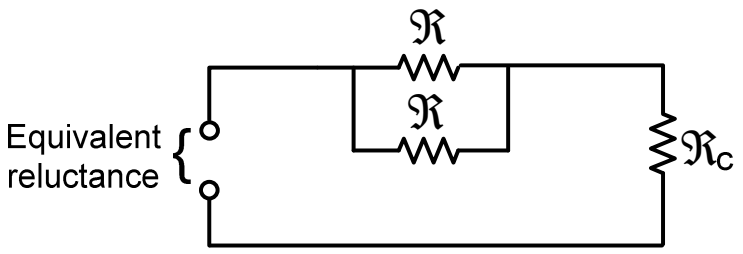

Fig. 9. Equivalent reluctance.

It is clear from this figure that the equivalent reluctance is equal to

$$\Re_{reverse(1-2)}(\text{with 3-4 shorted}) = \Re_c + (\Re \,||\, \Re) = \Re_c + 0.5\Re \tag{8}$$

Knowing that $L=N^2/R$, and using (7) and (8) yields

$$L_{reverse(1-2)}(\text{with 3-4 shorted}) = 2L_k = \frac{N^2}{\Re_c + 0.5\Re}$$
$$\text{or} \tag{9}$$
$$L_k = \frac{N^2}{2\Re_c + \Re}$$

And using (9) to solve (2) yields

$$L_m = N^2 \frac{\Re_c}{2\Re\Re_c + \Re^2} \tag{10}$$

With the definition of Lk and Lm in terms of R and Rc, it would be possible to design a coupled inductor.

1.4 Previous work

The advantages of employing multiphase interleaved structure such as ripple cancellation have been presented in [1-4]. On the other hand, multiphase interleaving increases the number of inductors compared to the conventional converter. One way to overcome these shortcomings is to use coupled magnetic components, which reduces the core number and complexity of the converters [5]. Multiphase interleaved boost converter has been studied for application to power-factor correction circuits [6-9] and high-power distributed conversion systems [3, 10]. The interleaved boost converter is composed of several identical boost converters connected in parallel and each converter is controlled by interleaved switching signals which have the same switching frequency and the same phase shift. An interleaved boost converter with high reliability and efficiency can be realized by sharing the input current among paralleled converters [1, 10]. Also, the interleaved boost converter exhibits both lower current ripple at the input side and lower voltage ripple at the output side as a consequence of the interleaving operation, so that the size and losses of the filtering stages can be significantly reduced [10]. A number of research results have been reported for the two-phase interleaved boost system [11 – 13]. When the two-phase interleaved boost converter operates in the continuous conduction mode and with a duty ratio of 50%, the converter acts as a voltage doubler and reveals a loss-free resistor characteristic. Sliding-mode control has been employed to guarantee a duty cycle of 50% with equal distribution of current between two inductors [11, 12]. Some converter performance expressions and transfer functions have been derived when the inductors are coupled [13-19].

1.5 Research objective

The objective of this thesis is to investigate the benefits of applying coupled inductors to multiphase DC-DC converters. Two different coupling methods, direct coupling and inverse coupling, will be applied to multiphase interleaved boost converter, respectively. An application of directly coupled inductors to multiphase DC-DC converters for further reducing the overall current ripple will be explored. Detailed mathematical analysis of overall current ripple and phase current ripple of the converter will be done. The proposed system will be designed and roughly tested by means of computer simulations. Then an experimental prototype will be built and tested to validate the concept. Also the use of inversely coupled inductors to multiphase DC-DC converters will be investigated. Analysis will be done on searching for the relationship between current ripples of the system and operating conditions, such as duty cycle and coupling coefficient. The system will be designed based on the concept and tested by computer simulations. Then experimental prototype will be built and tested to demonstrate the concept. Small-signal models of multiphase boost converters with uncoupling, direct coupling and inversely coupling will be compared. Based on the small-signal models, digital control scheme will be designed using digital redesign method and finally implemented in FPGA board [20]. Then new structure using coupled inductors will be proposed to improve the performance, which will be demonstrated by computer simulations.

1.6 Thesis outline

This thesis is composed of five chapters.

Chapter I introduces the research background of multiphase DC-DC converters and reviews some basic concepts of coupled inductors, including approaches to measure coupled inductor parameters and equating reluctance model and electric model of coupled inductors. Previous work on this topic is discussed and then the research objective of this work is presented.

Chapter II discusses multiphase DC-DC converters with directly coupled inductors. Detailed operation analysis is done based on a two-phase boost converter. A generalized model of N-phase interleaved boost converter is derived. The advantages and disadvantages of directly coupled inductor are discussed and demonstrated by simulation results and experimental results.

Chapter III discusses and analyzes the application of inversely coupled inductors for multiphase DC-DC converters. Operation principles are first discussed to show inversely coupled inductors can be used to improve the performance of multiphase DC-DC converters. Small-signal models of multiphase boost converter with different coupling methods are compared. Digital control loop is designed based on digital redesign method and implemented in FPGA board. Simulation and experimental results are shown to validate the concept.

Chapter IV proposes a new structure for multiphase DC-DC converters using coupled inductors. A 4-phase interleaved buck converter with proposed structure is analyzed. The advantages of this new structure will be discussed and demonstrated by computer simulations.

Chapter V summarizes this work and proposes ideas for future work.

CHAPTER II
MULTIPHASE DC-DC CONVERTERS WITH DIRECTLY COUPLED INDUCTORS

2.1 Introduction

A distributed energy system consisting of fuel cell, battery and possibly other energy storage components can be used in electric vehicles and stationary power system applications, which normally require a boost converter for energy management that employs an energy storage component to assist the slow-responding fuel cell [21, 22]. Multiphase structure with interleaved control is essential for the boost converter in order to reduce the ripple current and to reduce the size of passive component. On the other hand, although parallel individual DC-DC converters in interleaved structure have been demonstrated to reduce the overall current ripple, it is still challenging to meet today's requirements. In addition, the multiphase interleaving structure has more inductors than the single phase converters, which increases the complexity of this converter. Solution has to be found to reduce the core number and the complexity of converters. This chapter is aimed to improve the performance of multiphase DC-DC converters by employing directly coupled inductors.

2.2 Overall current ripple reduction with directly coupled inductors

Fig. 10 shows the schematic diagram of the two-phase interleaved boost converter with directly coupled inductors. The coupled inductors L1 and L2 share the same winding orientation.

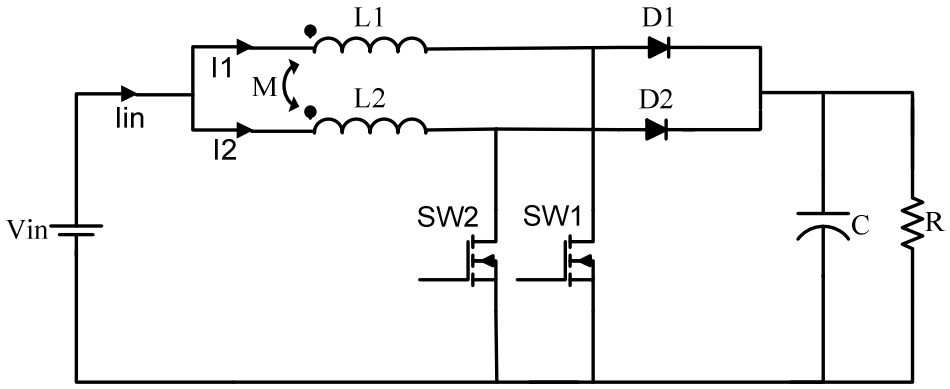

Fig. 10. Two-phase boost converter with directly coupled inductors.

Fig. 11 shows the equivalent model of directly coupled inductors, where Lk1 and Lk2 are the leakage inductance, and Lm is the mutual inductance.

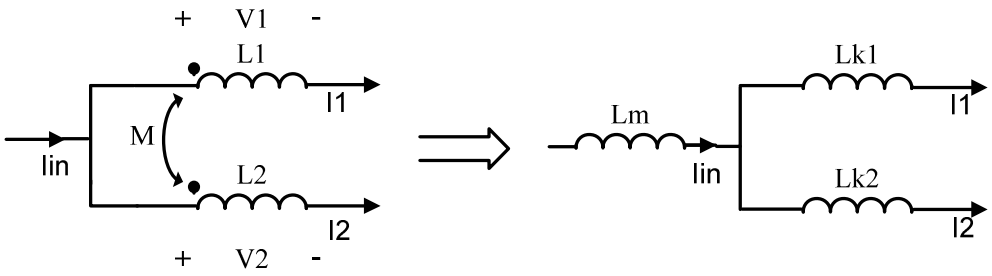

Fig. 11. Equivalent model of directly coupled inductors.

The relationships of the coupled inductors are

$$\begin{aligned} Lk1 &= L1 - Lm \\ Lk2 &= L2 - Lm \\ Lm &= \alpha\sqrt{L1L2} \end{aligned} \tag{11}$$

where L1,L2 is inductances of the two inductors, α is the coupling coefficient, Lk1,Lk2 are leakage inductances of the two inductors in the equivalent circuit, Lm is mutual inductance. For convenience of analysis, we set L1=L2=L and Lk1=Lk2=Lk.

Assume the voltage across the coupled inductors L1, L2 is V1 and V2, respectively, it can be found

$$\begin{aligned} V1 &= L\frac{dI1}{dt} + Lm\frac{dI2}{dt} \\ V2 &= L\frac{dI2}{dt} + Lm\frac{dI1}{dt} \end{aligned} \tag{12}$$

After rearranging (12), we can derive

$$\begin{aligned} V1 - \frac{Lm}{L}v2 &= (L - \frac{Lm^2}{L})\frac{dI1}{dt} \\ V2 - \frac{Lm}{L}v1 &= (L - \frac{Lm^2}{L})\frac{dI2}{dt} \end{aligned} \tag{13}$$

Fig.12 shows the gating signal during one general switching cycle, where VG1 and VG2 are the gating signals of SW1 and SW2, respectively.

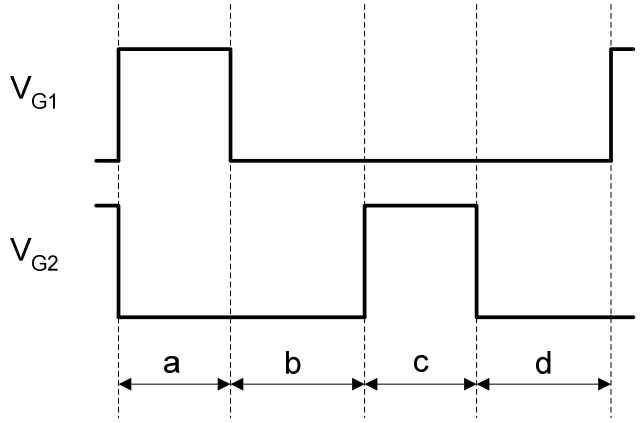

Fig. 12. One general switching cycle.

During time interval a, SW1 is on and SW2 is off, hence V1 and V2 can be found as

$$\begin{aligned} V1 &= Vin \\ V2 &= Vin - Vo \end{aligned} \tag{14}$$

Based on (14), and also according to Vo/Vin=1/(1-D), we can reach

$$V2 = -\frac{D}{1-D} V1 \tag{15}$$

Substituting (15) into (13) yields (16)

$$V1 = \frac{L - \frac{Lm^2}{L}}{1 + \frac{Lm}{L} \cdot \frac{D}{1-D}} \frac{dI1}{dt} \tag{16}$$

According to (16), when the mutual inductance Lm is equal to 0, which means uncoupling, the corresponding equation becomes

$$V1 = L \frac{dI1}{dt} \tag{17}$$

By comparing (16) and (17), we can get the equivalent inductance during state a as

$$Leq, a = \frac{L - \frac{Lm^2}{L}}{1 + \frac{Lm}{L} \cdot \frac{D}{1-D}} = \frac{1-\alpha^2}{1 + \alpha \cdot \frac{D}{1-D}} L \tag{18}$$

During time interval b, V1 and V2 are found as

$$\begin{aligned} V1 &= Vin - Vo \\ V2 &= Vin - Vo \end{aligned} \tag{19}$$

Therefore, V1 and V2 have the relationship of

$$V1 = V2 \tag{20}$$

Substituting (20) into (13) we can reach

$$Leq, b = (1+\alpha)L \tag{21}$$

Similarly, during time interval c, V1 and V2 are

$$V1 = Vin - Vo$$
$$V2 = Vin \tag{22}$$

Therefore, V1 and V2 have the relationship of

$$V2 = -\frac{1-D}{D} V1 \tag{23}$$

Substituting (23) into (13) we can reach

$$Leq,c = \frac{1-\alpha^2}{1+\alpha \cdot \frac{1-D}{D}} L \tag{24}$$

During state d, V1 and V2 become

$$V1 = Vin - Vo$$
$$V2 = Vin - Vo \tag{25}$$

Therefore, V1 and V2 has the relationship of

$$V1 = V2 \tag{26}$$

Substituting (26) into (13) we can reach

$$Leq,d = (1+\alpha)L \tag{27}$$

which is same as the equivalent inductance in time interval b.

The phase current and overall current waveforms under the condition of duty cycle less than 0.5, is shown in Fig.13. The one with dashed lines is the case with uncoupled inductors, while solid lines represent current waveforms of directly coupled inductors. It can be seen from Fig.13 that Leq,a always determines the peak to peak phase current ripple.

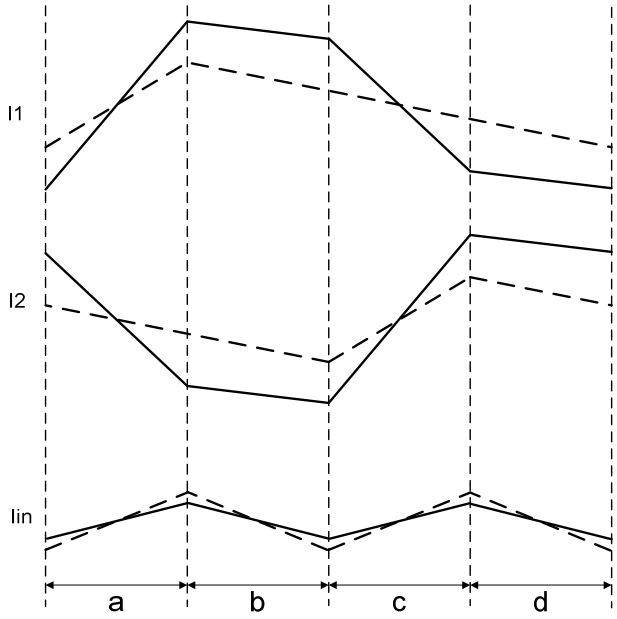

Fig. 13. Current waveforms in one general switching cycle. (α=0.61, D=0.25)

Therefore, during state a, the ripples of phase current I1 and I2 can be found as

$$\Delta I1,a=\frac{VinDT}{Leq,a}=\frac{VinDT}{L}\frac{1+\alpha\cdot\frac{D}{1-D}}{1-\alpha^2} \tag{28}$$

$$\Delta I2,c=\frac{(Vin-Vo)DT}{Leq,c}=-\frac{VinDT}{L}\frac{\alpha+\frac{D}{1-D}}{1-\alpha^2} \tag{29}$$

The overall input current ripple is the sum of the ripple currents of phase 1 and phase 2, which can be derived as

$$\Delta Iin,dir=\Delta I1,a+\Delta I2,c=\frac{VinDT}{L}\frac{1-2D}{1-D}\frac{1}{1+\alpha} \tag{30}$$

As for the case with uncoupled inductors, the input current can also be derived as

$$\Delta Iin,unc=\frac{VinDT}{L}+\frac{(Vin-Vo)DT}{L}=\frac{VinDT}{L}\frac{1-2D}{1-D} \tag{31}$$

Therefore, comparing (30) with (31), the ratio of input current with direct coupling and uncoupling can be found as

$$\frac{\Delta Iin, dir}{\Delta Iin, unc} = \frac{1}{1+\alpha} \tag{32}$$

It can be seen while α is equal to 0, which means uncoupling, the ratio becomes 1. While α is equal to 1, which means perfect direct coupling, the input current ripple can be reduced by half. Fig.14 shows overall current ripple comparison of uncoupling and direct coupling.

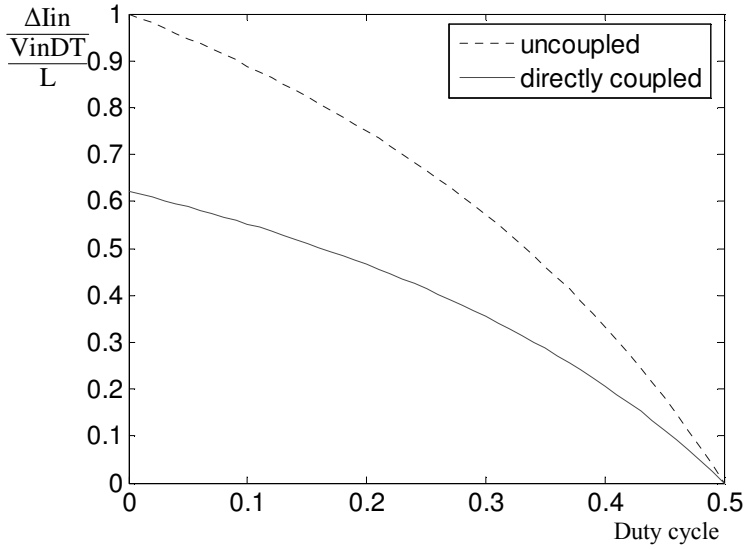

Fig. 14. Input current reduction with directly coupled inductors (α=0.61).

Although increasing the coupling coefficient α can effectively reduce the input current ripple, the phase current ripple will be increased. The ratio of phase current ripple with these two coupling methods can be derived as

$$\frac{\Delta I1, dir}{\Delta I1, unc} = \frac{1+\alpha \cdot \dfrac{D}{1-D}}{1-\alpha^2} \tag{33}$$

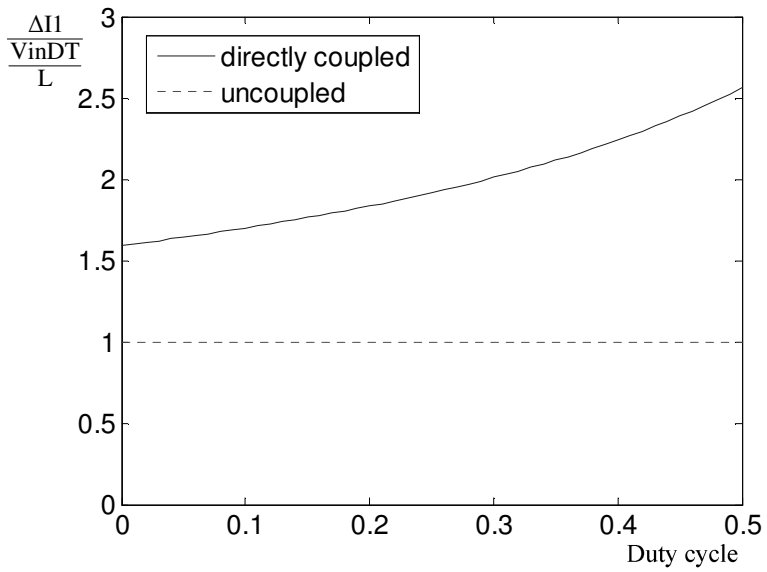

Fig. 15. Phase current increase with directly coupled inductors (α=0.61).

Fig.15 shows the increase of phase current ripple of directly coupled inductors, compared to that of uncoupled inductors. It can be seen the phase current ripple will increase with the coupling coefficient. Therefore, coupling coefficient α should be carefully chosen, in order to reduce the overall input current ripple while satisfying the phase current ripple limits.

2.3 Generalized expression of equivalent inductance

To obtain generalized expressions of equivalent inductance, N-phase boost converter with directly coupled inductors will be investigated. The voltage across each coupled windings can be found as

$$\begin{aligned} V1 &= L\frac{dI1}{dt} + Lm\frac{dI2}{dt} + ... + Lm\frac{dIn}{dt} \\ V2 &= Lm\frac{dI1}{dt} + L\frac{dI2}{dt} + ... + Lm\frac{dIn}{dt} \\ &\cdot \quad \cdot \quad \cdot \quad \cdot \quad \cdot \\ &\cdot \quad \cdot \quad \cdot \quad \cdot \quad \cdot \\ &\cdot \quad \cdot \quad \cdot \quad \cdot \quad \cdot \\ Vn &= Lm\frac{dI1}{dt} + Lm\frac{dI2}{dt} + ... + L\frac{dIn}{dt} \end{aligned} \tag{34}$$

In state 1, only SW1 is open, all other switches are closed, therefore

$$\begin{aligned} V1 &= Vin \\ Vk(k = 2...n) &= Vin - Vo \end{aligned} \tag{35}$$

Combining (35) with Vo/Vin=1/(1-D) gives

$$Vk(k = 2...n) = -\frac{D}{1-D}V1 \tag{36}$$

Based on (34), it can also be found

$$\sum_{k=2}^{n} Vk = (n-1)Lm\frac{dI1}{dt} + [L + (n-2)Lm]\sum_{k=2}^{n}\frac{dIk}{dt} \tag{37}$$

Substituting (36) into (37) and after rearrangement, it can be derived

$$\sum_{k=2}^{n}\frac{dIk}{dt} = \frac{(n-2)(-\frac{D}{1-D}V1) - (n-1)Lm\frac{dI1}{dt}}{L + (n-2)Lm} \tag{38}$$

Since

$$V1 = L\frac{dI1}{dt} + Lm\frac{dI2}{dt} + ... + Lm\frac{dIn}{dt} = L\frac{dI1}{dt} + Lm\sum_{k=2}^{n}\frac{dIk}{dt} \tag{39}$$

Substituting (38) into (39) yields

$$V1 = L\frac{dI1}{dt} + Lm\frac{(n-2)(-\frac{D}{1-D}V1) - (n-1)Lm\frac{dI1}{dt}}{L + (n-2)Lm} \tag{40}$$

Rearranging (40) gives

$$V1 = \frac{1 - \frac{Lm^2(n-1)}{L[L+(n-2)Lm]}}{1 + \frac{(n-1)Lm}{L+(n-2)Lm} \cdot \frac{D}{1-D}} \frac{dI1}{dt} \tag{41}$$

Therefore, the equivalent inductance during state 1 can be derived as

$$Leq,1 = \frac{1 - \frac{Lm^2(n-1)}{L[L+(n-2)Lm]}}{1 + \frac{(n-1)Lm}{L+(n-2)Lm} \cdot \frac{D}{1-D}} = \frac{1+(n-2)\alpha-(n-1)\alpha^2}{1+(n-2)\alpha+(n-1)\alpha\frac{D}{1-D}} L \tag{42}$$

In state 3, which means only SW2 is open and all other switches are closed, therefore

$$\begin{aligned} V2 &= Vin \\ Vk(k = 1,3...n) &= Vin - Vo \end{aligned} \tag{43}$$

Hence the relationship between V2 and Vk becomes

$$V2 = -\frac{1-D}{D} Vk(k = 1,3...n) \tag{44}$$

Based on (44), it is obvious

$$\frac{dI1}{dt} = \frac{dI3}{dt} = ... \frac{dIn}{dt} \tag{45}$$

Therefore,

$$V2 = L\frac{dI2}{dt} + (n-1)Lm\frac{dI1}{dt} \tag{46}$$

Substituting (44) into (46) and after rearranging yields

$$\frac{dI2}{dt} = \frac{-\frac{1-D}{D}V1 - (n-1)Lm\frac{dI1}{dt}}{L} \tag{47}$$

Since

$$V1 = L\frac{dI1}{dt} + Lm\frac{dI2}{dt} + ... + Lm\frac{dIn}{dt} = L\frac{dI1}{dt} + (n-2)Lm\frac{dI1}{dt} + Lm\frac{dI2}{dt} \tag{48}$$

Therefore, substituting (47) into (48) yields

$$V1 = L\frac{dI1}{dt} + (n-2)Lm\frac{dI1}{dt} + Lm\frac{-\frac{1-D}{D}V1 - (n-1)Lm\frac{dI1}{dt}}{L} \tag{49}$$

After rearranging (49) yields

$$V1 = \frac{L + (n-2)Lm - \frac{(n-1)Lm^2}{L}}{1 + \frac{Lm}{L}\frac{1-D}{D}}\frac{dI1}{dt} \tag{50}$$

Therefore, Leq,3 is found as

$$Leq,3 = \frac{L + (n-2)Lm - \frac{(n-1)Lm^2}{L}}{1 + \frac{Lm}{L}\frac{1-D}{D}} = \frac{1 + (n-2)\alpha - (n-1)\alpha^2}{1 + \frac{\alpha(1-D)}{D}} \tag{51}$$

Under the condition of D<1/n, the phase current ripple is decided by Leq,1.

$$\Delta I1,a = \frac{VinDT}{Leq,1} = \frac{VinDT}{L}\frac{1 + (n-2)\alpha + (n-1)\alpha\frac{D}{1-D}}{1 + (n-2)\alpha - (n-1)\alpha^2} \tag{52}$$

When phase 1 current is in state 1, current ripple of other phases is in state 3 and hence is decided by Leq,3.

$$\Delta I2,c = \frac{(Vin - Vo)DT}{Leq,3} = -\frac{VinDT}{L}\frac{\frac{D}{1-D} + \alpha}{1 + (n-2)\alpha - (n-1)\alpha^2} \tag{53}$$

Therefore, the overall input current ripple can be derived as

$$\Delta Iin = \Delta I1,a + \sum_{k=2}^{n}\Delta Ik,c = I1,a + (n-1)\Delta I2,c = \frac{VinDT}{L}\frac{(1-\alpha)[1-(n-1)\frac{D}{1-D}]}{1 + (n-2)\alpha - (n-1)\alpha^2} \tag{54}$$

Fig.16 and Fig.17 shows the normalized input current ripple and phase current ripple with different phase number. It can be seen under the condition of D<1/n, increasing the phase number can reduce the input current ripple while increasing the phase current ripple.

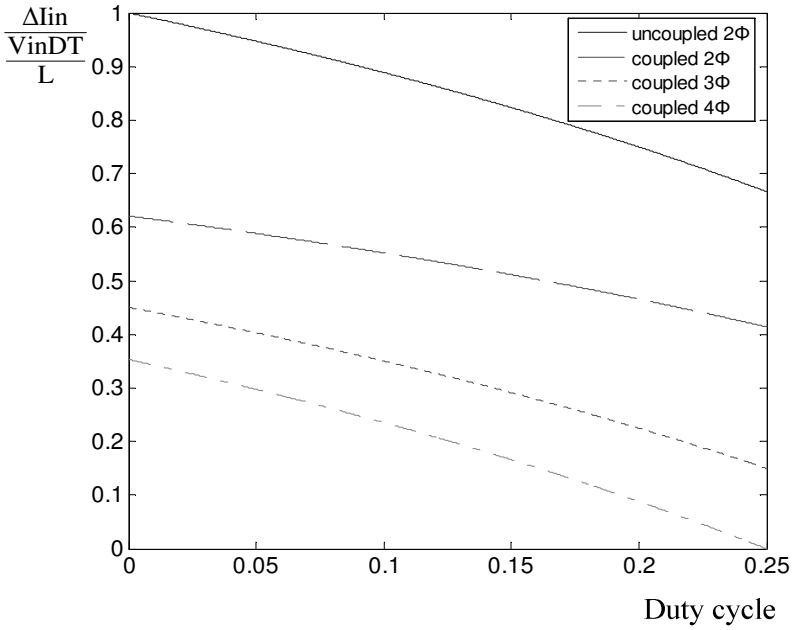

Fig. 16. Normalized input current ripple with different phase number.

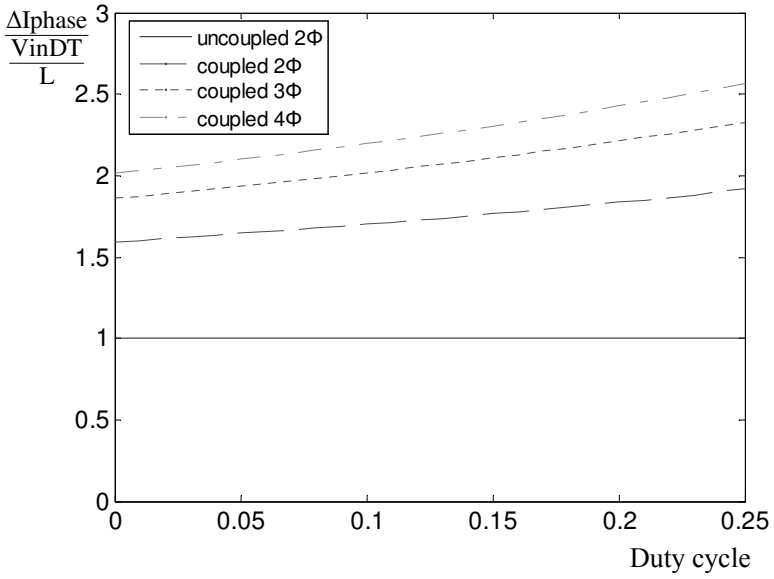

Fig. 17. Normalized phase current ripple with different phase number.

The derivation for equivalent inductances under the condition of D>1/n is similar therefore not done here.

2.4 Design example

The two-phase interleaved boost converter with directly coupled inductors is designed with input voltage of 5V while the output voltage is targeted at 6.25V with full load modeled as 4Ω. The duty cycle can be found as

$$D = 1 - \frac{Vin}{Vo} = 0.2 \tag{55}$$

Knowing power and input voltage, the input current is calculated to be 1.96A. Then the phase current is obtained as 0.98A. With 10% peak-to-peak phase current ripple and 20KHz switching frequency, minimum equivalent inductance Leq,a is calculated to be

$$Leq, a \geq \frac{VinDT}{\Delta Iphase} = 510.20\mu H \tag{56}$$

With a coupling coefficient of 0.61, the minimum self-inductance of the coupled inductor is found as

$$L \geq \frac{1 + \alpha \cdot \frac{D}{1-D}}{1-\alpha^2} Leq, a = 936.46\mu\text{H} \tag{57}$$

The self-inductance is chosen as 1000uH, and the mutual inductance Lm and leakage inductance Lk is calculated to be

$$\begin{aligned} Lm &= \alpha \cdot L = 610\mu\text{H} \\ Lk &= (1-\alpha) \cdot L = 390\mu\text{H} \end{aligned} \tag{58}$$

The steady state equivalent inductance Leq,a is obtained as

$$Leq,a = \frac{1-\alpha^2}{1+\alpha\cdot\dfrac{D}{1-D}} L = 544.82\mu H \tag{59}$$

This yields phase current ripple and input current ripple of

$$\begin{aligned} \Delta Iphase &= \frac{VinDT}{Leq,a} = 0.092A \\ \Delta Iin &= \frac{VinDT}{L}\frac{1-2D}{1-D}\frac{1}{1+\alpha} = 0.023A \end{aligned} \tag{60}$$

2.5 Simulation results

A two-phase interleaved boost converter with directly coupled inductors is simulated in PSIM. All the components including MOSFETs, diodes, coupled inductors are assumed to be ideal. The simulation parameters are summarized as Vin=5V, R=4ohm, C=47uF, f=20KHz, L1=L2=1000uH, Lm=610uH, Lk1=Lk2=390uH, D=0.2, α=0.61. According to (22), direct coupling of α=0.61 can reduce the input current ripple to 62%, compared to the case with uncoupling.

Fig.18 shows the current waveforms of direct coupling and uncoupling. With uncoupled inductors, the input current ripple is 0.038A. With direct coupling, the input current ripple is reduced to 0.023A. On the other hand, the phase current ripple increases from 0.05A with uncoupling to 0.092A with direct coupling.

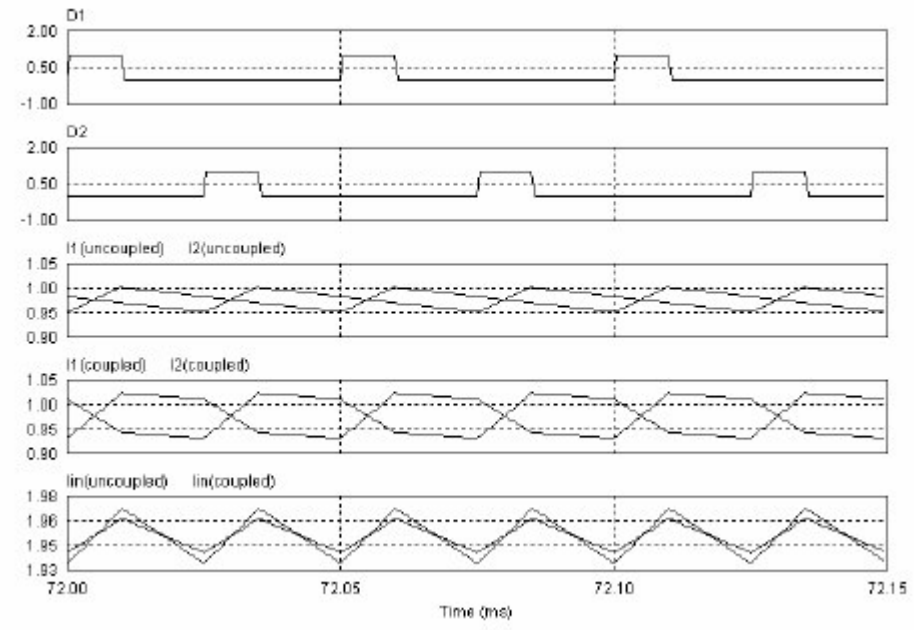

Fig. 18. Current waveforms with uncoupling and direct coupling.

2.6 Experimental results

Two-phase boost converters with uncoupled inductors and directly coupled inductors have been built and tested. Fig. 19 shows the experimentally measured current waveforms for the case with uncoupled inductors. The phase current ripple is measured to be 0.05A and input current ripple is measured to be 0.038 A. Fig.20 shows the current waveforms of the case with directly coupled inductors. The phase current is increased to 0.092A while the input current ripple is reduced to 0.024A.

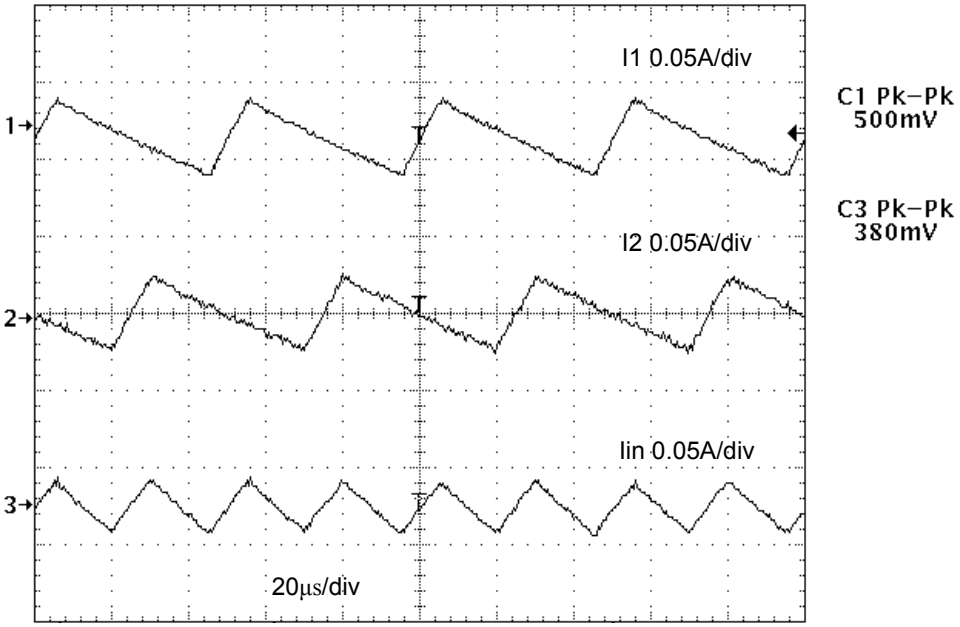

Fig. 19. Phase and input current ripple of uncoupled inductors.

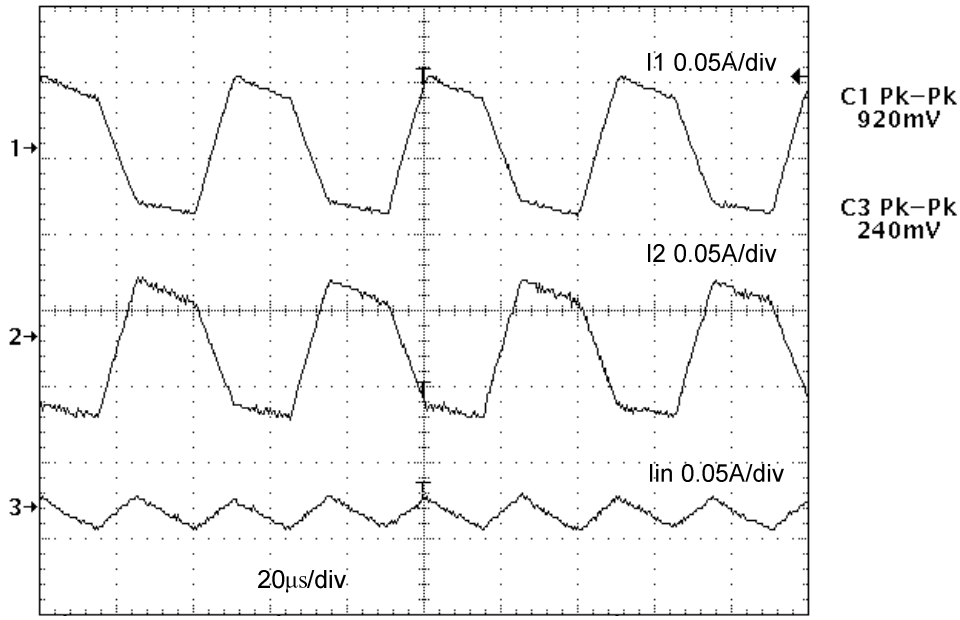

Fig. 20. Phase and input current ripple of directly coupled inductors.

2.7 Conclusions

This chapter presents the concept of overall current reduction of multiphase DC-DC converter by employing directly coupled inductors. Detailed analysis has been done while simulation and experimental results have been presented to validate the concept. In addition, it has been found that phase current ripple will also be increased, which may decrease the efficiency of the system. Therefore, direct coupling coefficient should be carefully chosen. For other multiphase DC-DC converters such as multiphase buck converter, the analysis is similar therefore not done here. It can be proven the output current ripple of multiphase buck converter with direct coupling can be reduced, which can result in less output voltage ripple. In other words, with same output voltage ripple requirement, using directly coupled inductors can lower output capacitance.

CHAPTER III
MULTIPHASE DC-DC CONVERTERS WITH INVERSELY COUPLED INDUCTORS

3.1 Introduction

Conventional power converters with multiphase interleaved structure have been proven that the overall current ripple can be effectively reduced, depending on the operating points. However, this benefit has not been extended to inductors and switches. In addition, in conventional multiphase DC-DC converters, current imbalance can occur due to the component tolerances or parameter variations. Therefore, those converters not only suffer from high ripple current on semiconductor devices, but also require individual phase currents sensed for current sharing purpose. Further, the conventional topology requires many magnetic cores. This chapter investigates the benefits of employing inversely coupled inductors to multiphase DC-DC converters. In addition, digital control loop compensation will be done based on small-signal model of multiphase DC-DC converters with inversely coupled inductor.

3.2 Operation analysis

The topology of two-phase interleaved boost converter with inversely coupled inductors is shown in Fig.21.

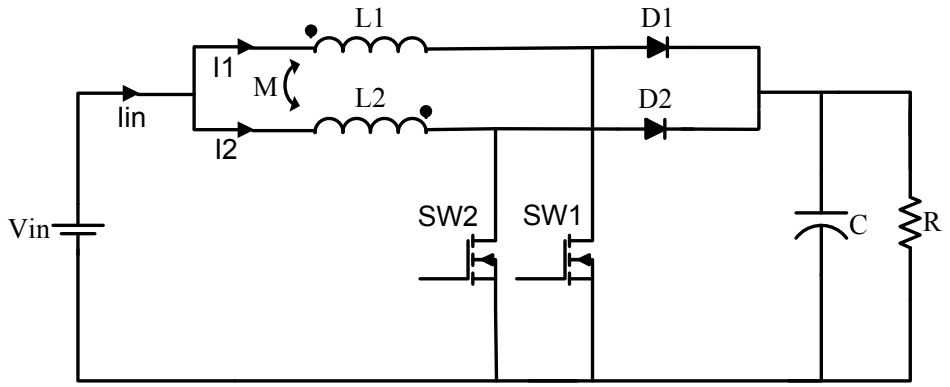

Fig. 21. Two-phase interleaved boost converter with inversely coupled inductors

The equivalent inductance analysis done in Chapter II for directly coupled inductors with D<0.5 still applies here. The analysis for duty cycle larger than 0.5 is similar to duty cycle smaller than 0.5, therefore not done here. It can be proven the equivalent inductances for duty cycle larger than 0.5 are exactly the same.

Under the condition of duty cycle less than 0.5 and in state a, the current ripples of phase 1, phase 2 and input current have the form of

$$\begin{aligned}
\Delta I1,a &= \frac{VinDT}{Leq,a} = \frac{VinDT}{L}\frac{1+\alpha\cdot\dfrac{D}{1-D}}{1-\alpha^2} \\
\Delta I2,a &= \frac{(Vin-Vo)DT}{Leq,c} = -\frac{VinDT}{L}\frac{\alpha+\dfrac{D}{1-D}}{1-\alpha^2} \\
\Delta Iin &= \Delta I1,a + \Delta I2,c = \frac{VinDT}{L}\frac{1-2D}{1-D}\frac{1}{1+\alpha}
\end{aligned} \tag{61}$$

Fig.22 shows the current waveforms of inversely coupled inductors compared to conventional uncoupled inductors.

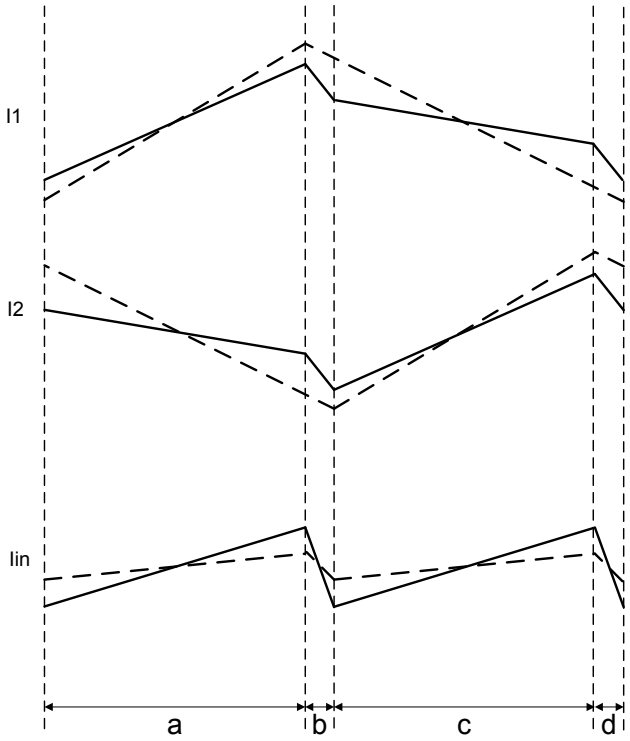

Fig. 22. Current waveforms with uncoupled inductors and inversely coupled inductors.

For example, under the condition of coupling coefficient α=-0.984, the peak to peak phase current ripple becomes

$$\Delta I1, pk-pk = \Delta I2, pk-pk = \frac{VinDT}{Leq,a} = \frac{VinDT}{L}\frac{1-0.984\cdot\frac{D}{1-D}}{1-0.984^2} \tag{62}$$

As for the input current ripple, it can be found as

$$\Delta Iin = \frac{VinDT}{L}\frac{1-2D}{1-D}\frac{1}{1-0.984} \tag{63}$$

Fig.23 shows normalized phase current ripple and overall input current ripple versus duty cycle. It can be seen when D=0.5, the normalized phase ripple current reaches the minimum 0.504.

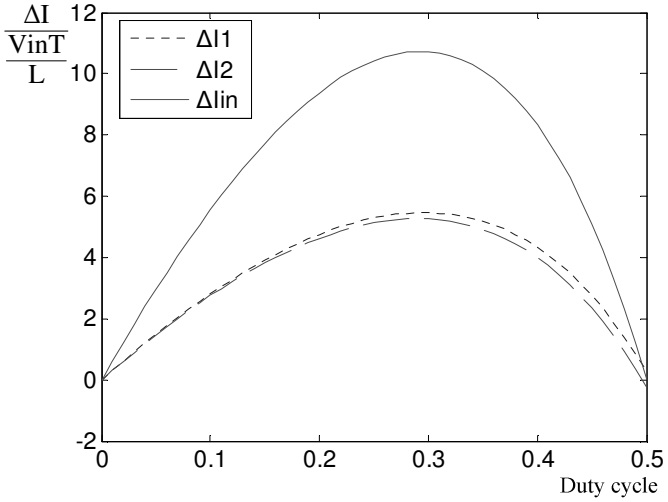

Fig. 23. Normalized current ripple.

Fig.24 shows the relationship between phase current ripple at different operating points and with different coupling coefficient. It can be found if the coupling coefficient is well chosen, the phase current ripple can be effectively reduced, compared to the uncoupled case.

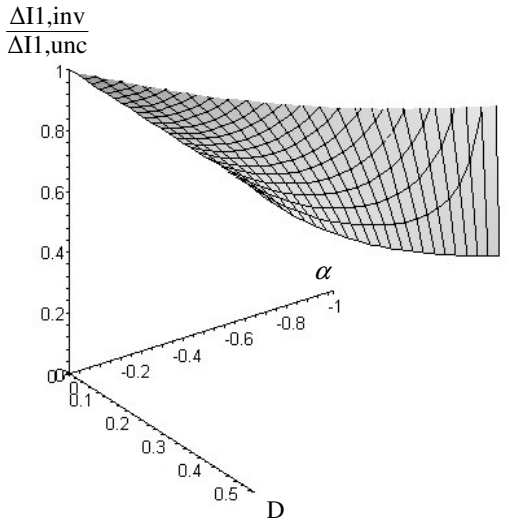

Fig. 24. Normalized phase current ripple with different operating points and α.

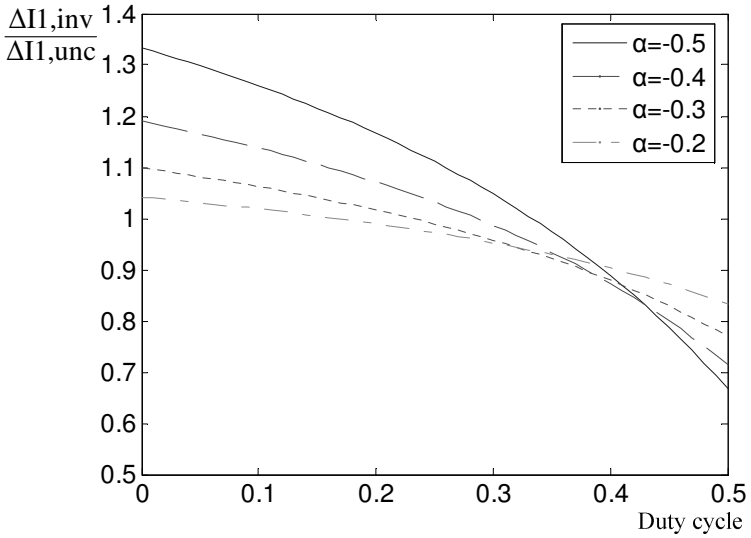

Fig. 25. Phase current ripple reduction with different coupling coefficient.

Fig.25 shows the phase current ripple can be reduced with carefully chosen coupling coefficient and operating points.

3.3 Design example

The system is designed to operate at 55W with input voltage of 10V. And the output voltage is targeted at 16.6V, which yields the duty cycle of

$$D = 1 - \frac{Vin}{Vo} = 0.4 \tag{64}$$

The resistance of the 55W load with the regulated output voltage is found to be

$$R = \frac{Vo^2}{P} = 5\Omega \tag{65}$$

Considering the efficiency of 85%, based on the output power and input voltage, the input current is calculated to be 4.68A. Therefore, the phase current is calculated to be

2.34A, and with 8% ripple and 40KHz switching frequency, minimum equivalent inductance Leq,a is calculated to be

$$Leq,a \geq \frac{VinDT}{2\Delta I} = 267.09uH \tag{66}$$

With a coupling coefficient of -0.984, the minimum self-inductance of the coupled inductor is found as

$$L \geq \frac{1+\alpha \cdot \frac{D}{1-D}}{1-\alpha^2} Leq,a = 2894.37\mu\text{H} \tag{67}$$

Then, the self-inductance is chosen as L=2970uH, and the mutual inductance Lm and leakage inductance Lk is calculated to be

$$\begin{aligned} Lm &= -\alpha \cdot L = 2922\mu\text{H} \\ Lk &= (1+\alpha) \cdot L = 48\mu\text{H} \end{aligned} \tag{68}$$

For 5% output voltage ripple, the minimal output capacitance is found to be

$$C \geq \frac{VoDT}{R\Delta Vo} = 40\mu F \tag{69}$$

Then, a 47uF capacitor is chosen.

3.4 Control loop design

For general two-phase interleaved boost converter working in continuous conduction mode, the control-to-output transfer function has the form of

$$G_{vd}(s) = \frac{Vin}{(1-D)^2} \times \frac{1-\frac{s}{\omega_{RHP}}}{(\frac{s}{\omega_o})^2 + \frac{s}{\omega_o Q} + 1} \tag{70}$$

where

$$\omega_{RHP} = \frac{R \times (1-D)^2}{L_{cm}}$$
$$\omega_o = \frac{1}{\sqrt{\frac{L_{cm}}{(1-D)^2} \times C}}$$
$$Q = R\sqrt{\frac{C}{\frac{L_{cm}}{(1-D)^2}}} \quad (71)$$
$$L_{cm} = \frac{L_k}{4}$$

Fig 26 shows the root locus of the control-to-output transfer function of the system. The parameters used are mutual inductance 2922uH, leakage inductance 48uH, output capacitor 47uF, switching frequency 40KHz, load resistance 5Ω, input voltage 10V. It can be seen that the transfer function has a pair of complex conjugate poles and a right-half-plane zero. Same as left-half-plane zero, right-half-plane zero increases the gain. But at the same time the phase angle will decrease, which is opposite to the function of left-half-plane zero. If the overall open-loop phase angle drops sufficiently low, the system can become unstable because of this RHP zero. That is why this zero is considered undesirable. Unfortunately, it is virtually impossible to compensate for it. The only solution is to push this RHP zero to higher frequencies where it can not affect the overall loop significantly.

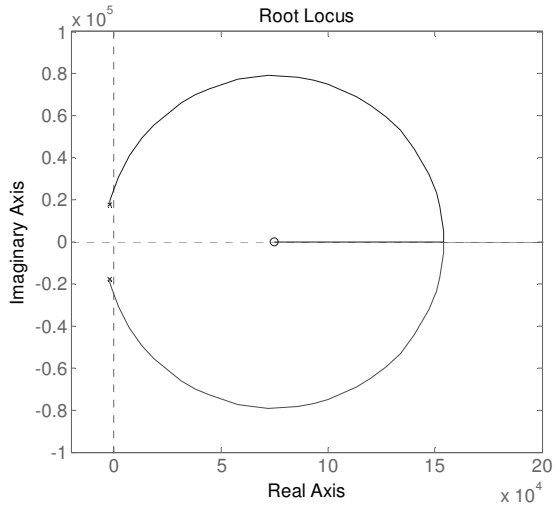

Fig. 26. Root locus.

As the control loop has to be implemented in FPGA board, digital compensator has to be employed. Digital compensator can be designed by either digital redesign method or direct digital method [23-25]. For direct digital design method, first the discrete form of the control-to-output transfer function has to be found. After the discrete model has been obtained, the digital compensator can be designed in z-domain directly. Either frequency response method or root-locus method can be used. For digital redesign method, the control loop is first designed in the continuous domain, which is similar to conventional analog control loop design. Then the equivalent discrete-time model can be obtained by one of the approximation techniques, such as bilinear approximation, impulse invariant discretization, matched pole-zero method and etc.

Fig.27 shows the bode plot of control-to-output response of the system.

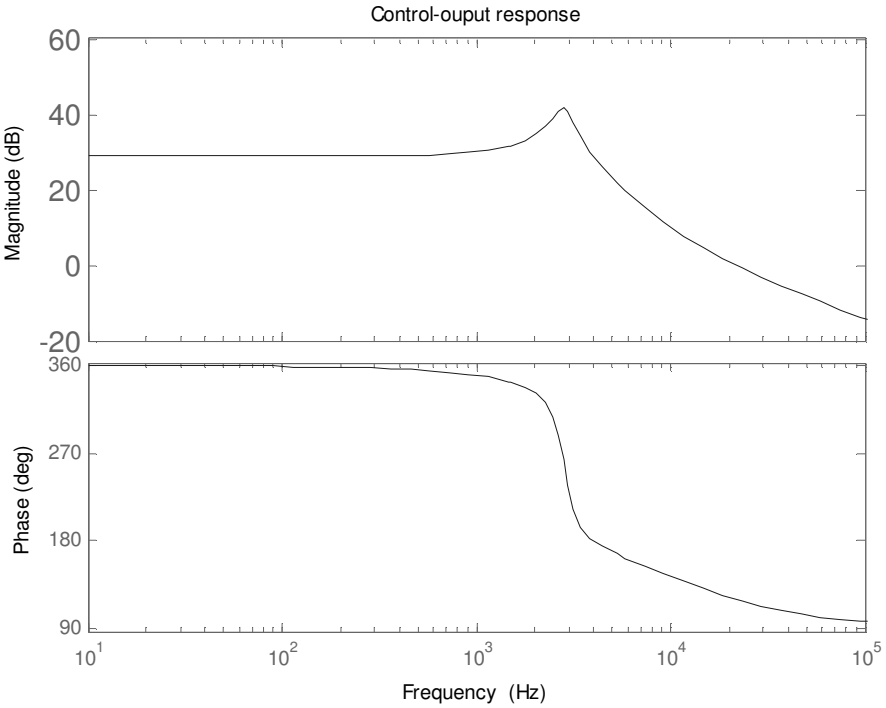

Fig. 27. Control-to-output response.

Two-pole two-zero method is used to compensate for the control loop, which yields the compensator as

$$G_c(s) = \frac{1.67s^2 + 1.57\times10^4 s + 5.23\times10^8}{s^2 + 3.98\times10^5 s} \tag{72}$$

Fig.28 shows the bode plot of the open loop gain. With compensation, the system becomes stable with bandwidth of 7KHz and phase margin of 45.6 degrees.

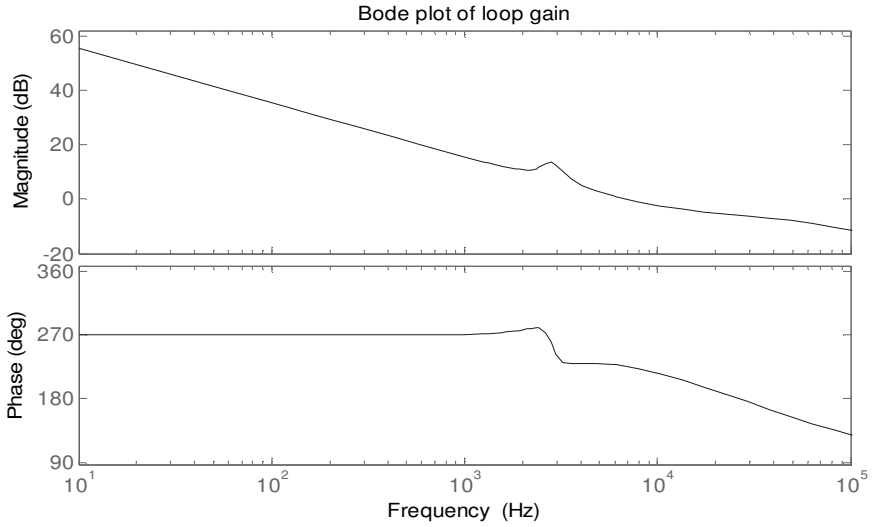

Fig. 28. Bode plot of loop gain.

With matched pole-zero method, we can convert the compensator from continuous domain to z-domain. The transfer function of the digital compensator is obtained as

$$G_c(z) = \frac{U}{E} = \frac{0.19 - 0.32z^{-1} + 0.13z^{-2}}{1 - z^{-1}} \tag{73}$$

which can be expressed as difference equation as

$$U(n) = U(n-1) + 0.19E(n) - 0.32E(n-1) + 0.13E(n-2) \tag{74}$$

where U(n) is the compensator output of the nth sample, and E(n) is the voltage error of the nth sample.

3.5 Simulation results

A two-phase interleaved boost converter with inversely coupled inductors is simulated. The parameters are mutual inductance 2922uH, leakage inductance 48uH, coupling coefficient -0.984, output capacitance 47uF, switching frequency, load resistance 5Ω, input voltage 10V. The simulation results are shown in Fig.29 (D=0.4) and

Fig.30 (D=0.28). For D=0.4, during state a, which means SW1 is on and SW is off, current ripples of phase 1 and phase 2 are 0.362A, 0.333A, respectively. And the input current ripple is 0.695A. While for D=0.28, the phase current ripples becomes 0.454A for phase 1 and 0.437A for phase 2. And the input current ripple increases to 0.891A.

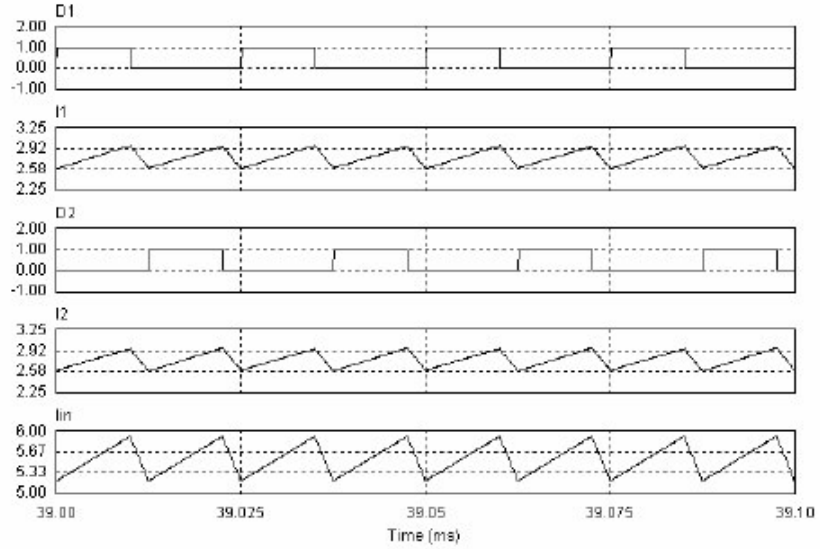

Fig. 29. Current waveforms with inversely coupled inductors (D1=D2=0.4).

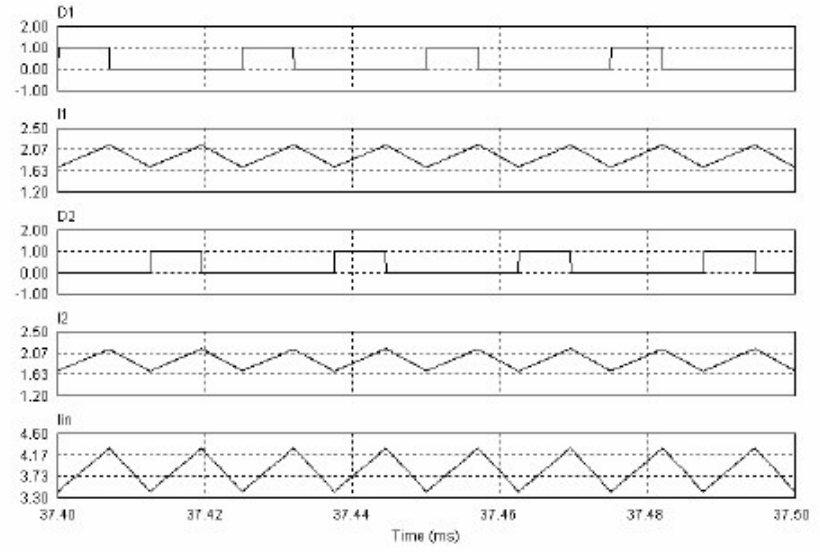

Fig. 30. Current waveforms with inversely coupled inductors (D1=D2=0.28).

3.6 Experimental results

An experimental prototype circuit has been built to validate the concepts and simulation results. The experimental results are given in Fig.31 and Fig.32, which show the gating signals and phase current ripples of the interleaved boost converter.

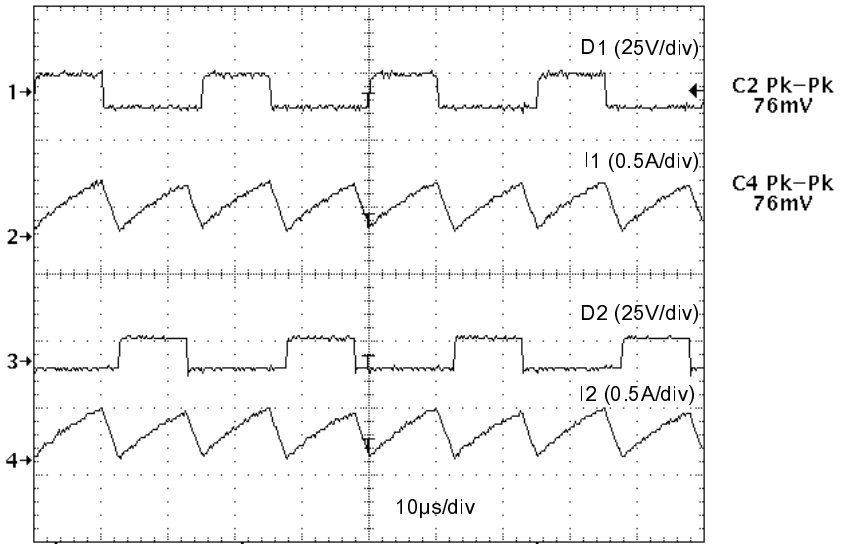

Fig. 31. Current waveforms with inversely coupled inductors (D1=D2=0.4).

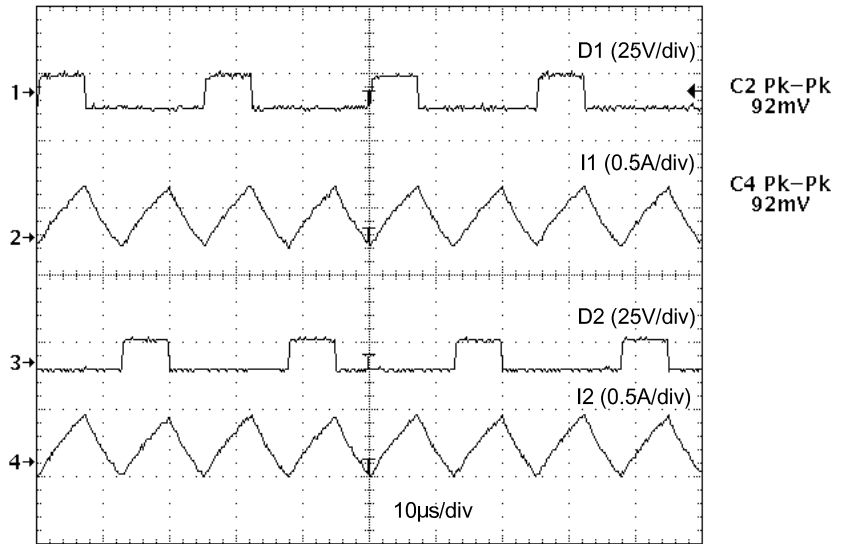

Fig. 32. Current waveforms with inversely coupled inductors (D1=D2=0.28).

As can be seen from Fig.31, under the condition of D1=D2=0.4, the phase current ripple is 0.38A. While according to Fig.32, the ripples increase to 0.46A when the operating point is changed to D1=D2=0.28.

3.7 Comparison of three coupling methods

For two-phase boost converter with uncoupled inductors (α=0), directly coupled inductors (α>0) and inversely coupled inductors (α>0), the general form of phase current ripple and input current ripple can be represented by

$$\begin{aligned} \Delta Iphase &= \frac{VinDT}{L}\frac{1+\alpha\cdot\frac{D}{1-D}}{1-\alpha^2} \\ \Delta Iin &= \frac{VinDT}{L}\frac{1-2D}{1-D}\frac{1}{1+\alpha} \end{aligned} \tag{75}$$

Based on (75), it can be seen for directly coupled inductors (α>0), phase current ripple will definitely increase while input current ripple will definitely decrease in any operating point, compared to those of uncoupled inductors. As for inversely coupled inductors, the input current ripple will definitely increase, while the phase current ripple may increase or decrease, depending on operating points and coupling coefficient α.

Fig.33 shows the normalized phase current ripple with uncoupling, direct coupling and inverse coupling. It can be seen for directly coupled inductors, increasing coupling coefficient results in larger phase current ripple, while for inversely coupled inductors, increasing coupling coefficient will broaden the range of operating points for phase current ripple reduction.

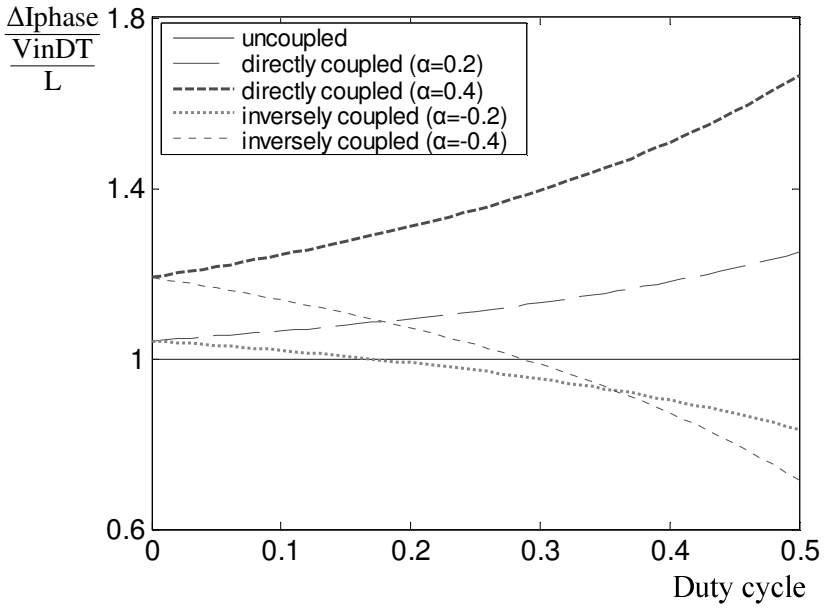

Fig. 33. Normalized phase current ripple comparison of different coupling methods.

Fig.34 shows the normalized input current ripple with three different coupling methods. For directly coupled inductors, by choosing larger coupling coefficient, input current ripple can be more effectively reduced. For inversely coupled inductors, larger coupling coefficient results in smaller input current ripple.

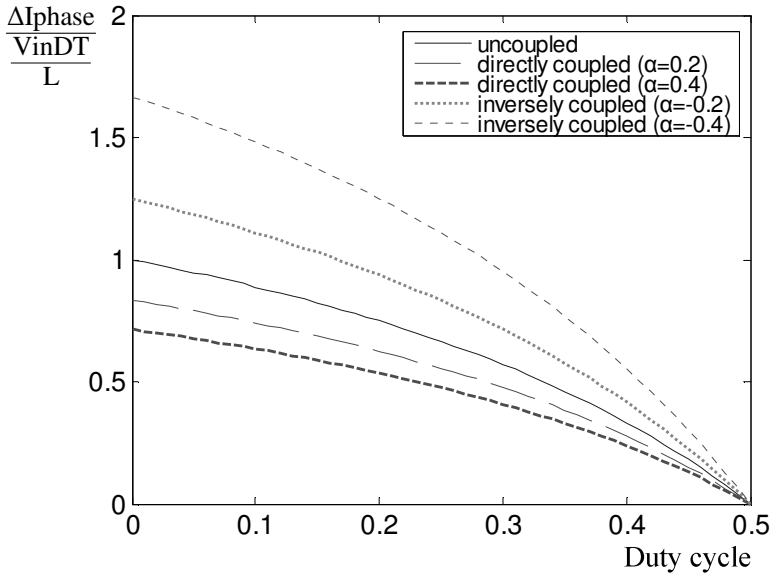

Fig. 34. Normalized input current ripple comparison of different coupling methods.

Table I shows the comparison of current ripple of inverse coupling and direct coupling in two-phase boost converter, compared to that of uncoupling.

Table I. Current ripple comparison

	direct coupling	inverse coupling
Phase current ripple	increase	increase or decrease
Overall current ripple	decrease	increase

The equivalent common-mode inductance of multiphase interleaved boost converter with different coupling methods has the general form of

$$L_{cm} = \frac{L_k}{2N} + \frac{1}{2}(1+\rho)L_m \tag{76}$$

where N is the phase number.

For inversely coupled inductors, ρ=-1, which yields

$$L_{cm,\,inv} = \frac{L_k}{2N} \tag{77}$$

For uncoupled inductors, ρ=0, and the common-mode inductance becomes

$$L_{cm,\,unc} = \frac{L_k}{2N} + \frac{L_m}{2} \tag{78}$$

As for directly inductors, ρ=1, which leads to

$$L_{cm,\,dir} = \frac{L_k}{2N} + L_m \tag{79}$$

Fig.35 shows the bode plot of control-to-output transfer function of three different types of inductor couplings. According to (77), inversely coupled inductors always have a smaller common-mode inductance Lcm than directly coupled inductors and uncoupled inductors. Therefore, the dynamics of inverse coupling are faster than other couplings. The dynamics of directly coupled inductors are slower to that of the uncoupled inductors according to (78) and (79).

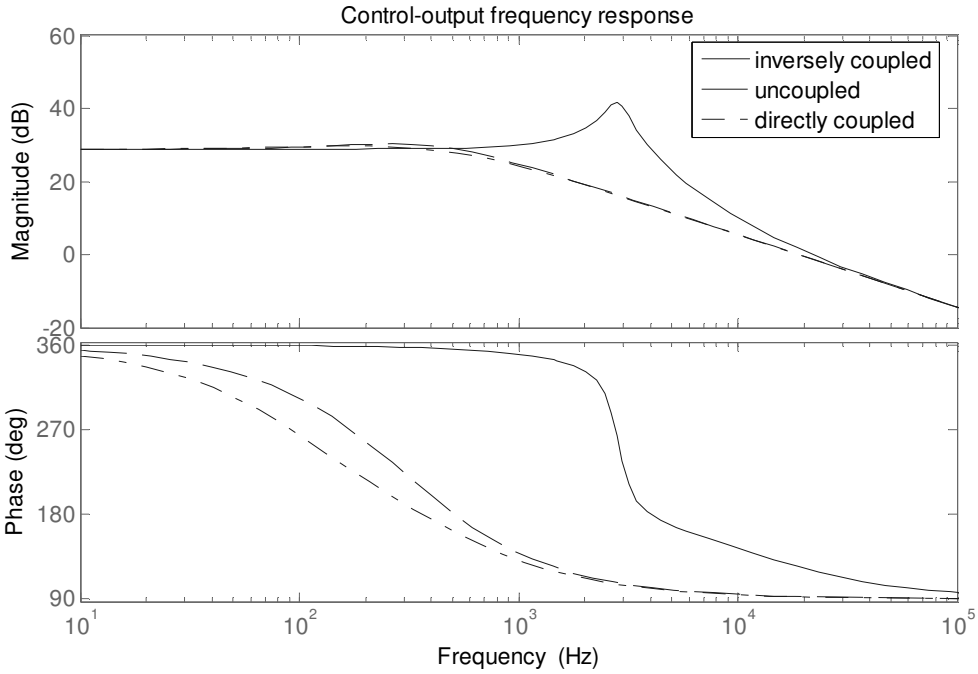

Fig. 35. Control-to-output response comparison.

The line-to-output transfer function Gvg has the forms of

$$G_{vg}(s) = \frac{1}{1-D} \times \frac{1}{(\frac{s}{\omega_o})^2 + \frac{s}{\omega_o Q} + 1} \tag{80}$$

Fig.36 shows the bode plot of line-to-output transfer functions according to three different coupling methods. At the low-frequency range, the performance of input disturbance does not depend on the inductor coupling methods. The corner frequencies are the same as that of the control-to-output transfer functions. For a line disturbance with higher frequency, inversely-coupled inductors yield the worst line regulation than directly coupled inductors and uncoupled inductors.

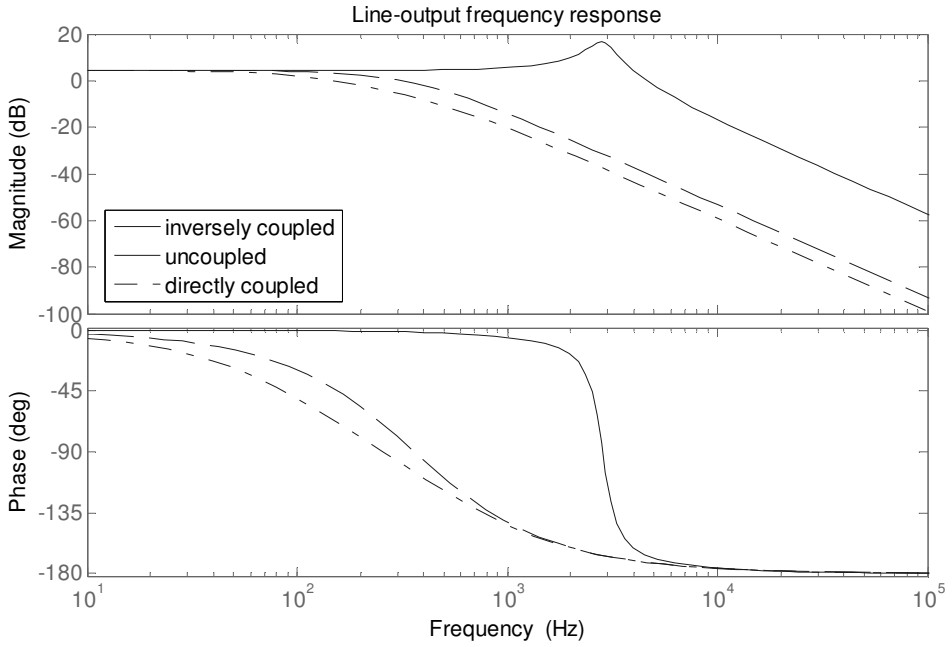

Fig. 36. Line-to-output response comparison.

The output impedance Zout has the form of

$$Z_{out}(s) = \frac{1}{C} \times \frac{s}{s^2 + \frac{1}{RC}s + \frac{(1-D)^2}{L_{eq}C}} \tag{81}$$

Fig.37 shows the output impedances according to the coupling method. At high frequencies the inductor coupling method has little effect on the frequency responses. The output impedance reaches the maximum at the corner frequency, which causes the load regulation worse in the range near the corner frequency. At middle frequency, the output voltage of the converter with inverse coupling is least sensitive to the load variation than directly coupling and uncoupling.

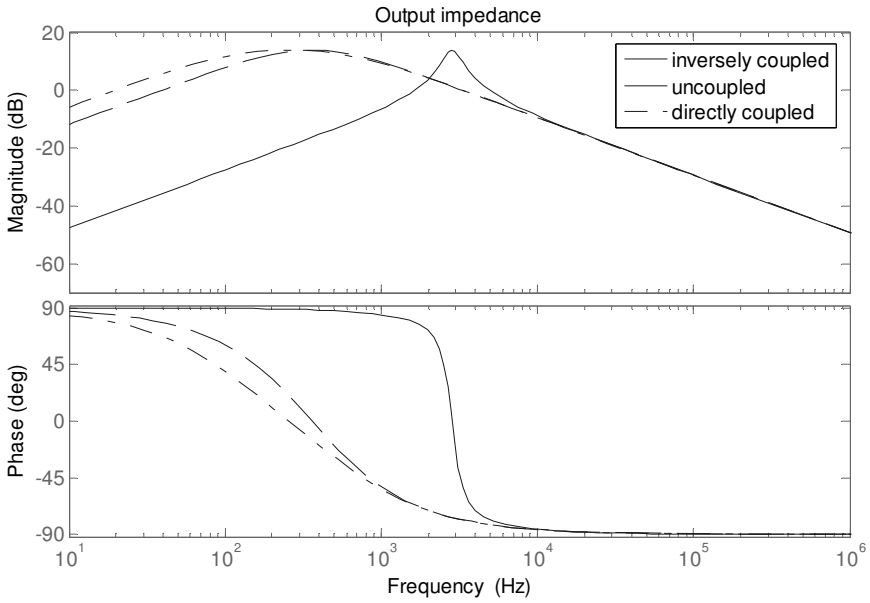

Fig. 37. Output impedance comparison.

Table II summarize the small-signal characteristics according to different coupling methods.

Table II. Small-signal characteristics according to different coupling methods

	uncoupling	direct coupling	inverse uncoupling
Bandwidth	Middle	Low	High
Sensitivity to input variation (Low frequency)	Similar	Similar	Similar
Sensitivity to input variation (high frequency)	Middle	Low	High
Sensitivity to load variation (Low frequency)	Middle	High	Low
Sensitivity to load variation (high frequency)	Similar	Similar	Similar

3.8 Application to fuel cell system

A distributed energy source consisting of a fuel cell normally requires a high-power boost converter for energy management to assist the slow-responding fuel cell. The high power boost converter is an essential interface between the fuel cell and the dc bus that serves as the inverter input.

A major design aspect in a high power boost converter is the selection of the boost inductor. The major concern is the size and weight of high power inductor. In order to reduce the inductor size and weight, a small inductance value is preferred. Multiphase structure with interleaved control is essential for the high-power boost converter in order to reduce the ripple current and to reduce the size of passive component. To further reduce the phase ripple current with the same inductance value, inversely coupled inductor can be employed, with appropriately chosen coupling coefficient and operating point. In other words, with the same phase current ripple requirement, the inductance of inversely coupled inductors can be reduced, compared to uncoupled inductors, hence reducing the size of magnetic components.

Another concern is high input current ripple is highly objectionable for a fuel-cell type source. In order to reduce the input current ripple, the converter can be designed with multiple legs interleaving each other allowing for ripple cancellation. Directly coupled inductors can be employed to further reduce the input current ripple. The input current ripple reduction of directly coupled inductors compared to uncoupled inductors has been derived as

$$\frac{\Delta Iin, dir}{\Delta Iin, unc} = \frac{1}{1+\alpha} \tag{82}$$

Therefore, increasing the coupling coefficient can more effectively reduce the input current ripple.

3.9 Conclusion

The operation of multiphase boost converter with inversely coupled inductors are discussed and analyzed. Two-phase interleaved boost converter is taken as an example. The relationship between phase current ripple, input current ripple versus operating point and coupling coefficient is analyzed. It is demonstrated multiphase DC-DC converter can effectively reduce the overall current ripple by choosing better operating point. Control loop compensation is first done in continuous domain and then converted to digital counterpart, which is later implemented in FPGA board. Comparison of three different coupling methods is presented. Application of coupled inductors to fuel cell system has been discussed.

CHAPTER IV
NEW STRUCTURE FOR MULTIPHASE DC-DC CONVERTERS

4.1 Proposed new structure

Fig.38 shows the proposed structure for 4-phase interleaved buck converter.

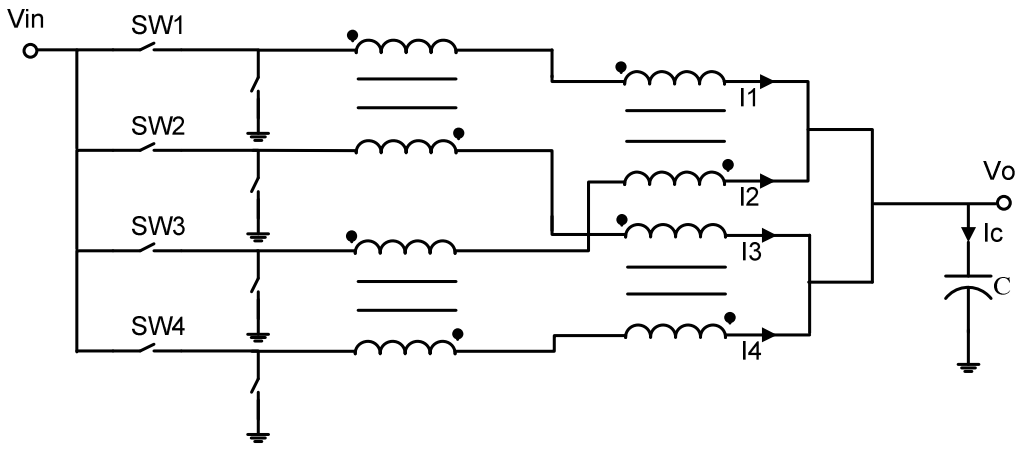

Fig. 38. Proposed new structure.

The equivalent model of the proposed structure is shown in Fig.39. The electrical circuit model of coupled inductor shown in this figure is comprised of an ideal transformer, magnetizing inductance Lm and leakage inductance Lk. This electrical circuit model can be used to model any linear magnetic structure with two windings.

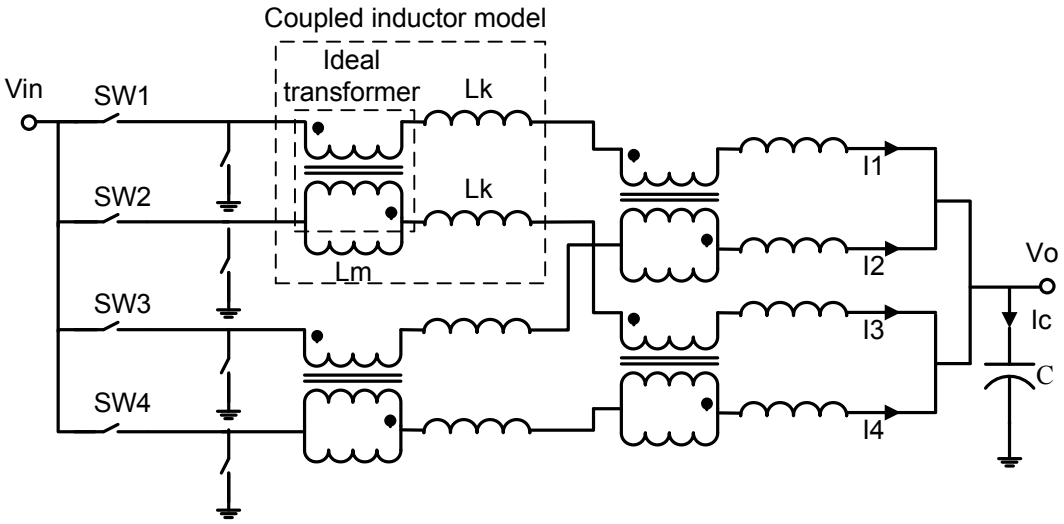

Fig. 39. Equivalent model.

With equal numbers of turns on the two windings, the ideal transformer has a 1:1 turns ratio. Leakage inductance and magnetizing inductance are affected by magnetic structures. For perfect coupling, magnetizing inductance approaches to infinity, hence Lm is approximately an open circuit for any ac currents or voltages.

As all four coupled inductors are same, all eight leakage inductances Lk are of the same value. Based on Fig.39, for those leakage inductances that are connected in series, they can be combined to one equivalent leakage inductance. Fig.40 simplifies the equivalent model of the proposed structure.

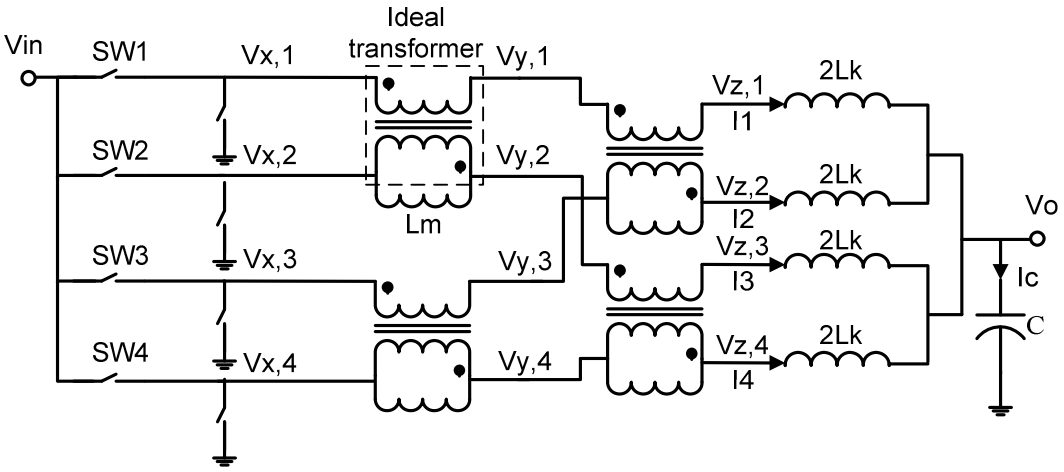

Fig. 40. Simplified equivalent model.

The ideal transformer (with the polarity as shown) forces the ac currents in the two phases to be equal. Thus the ac currents in the four equivalent leakage inductances, are also equal, assuming that the leakage inductances are equal. With equal ac currents, the leakage inductances also have identical voltages across them. Thus, the voltages at the nodes labeled Vz,1, Vz,2, Vz,3, Vz,4 must match.

Based on the transformer equation, it can be found

$$\begin{aligned} &Vx,1-Vy,1=Vy,2-Vx,2\\ &Vx,3-Vy,3=Vy,4-Vx,4\\ &Vy,1-Vz,1=Vz,2-Vy,3\\ &Vy,2-Vz,3=Vz,4-Vy,4 \end{aligned} \tag{83}$$

Rearranging (83) yields

$$\begin{aligned} &Vy,1+Vy,2+Vy,3+Vy,4=Vx,1+Vx,2+Vx,3+Vx,4\\ &Vy,1+Vy,2+Vy,3+Vy,4=Vz,1+Vz,2+Vz,3+Vz,4 \end{aligned} \tag{84}$$

Based on (84), it can be found

$$Vz,1+Vz,2+Vz,3+Vz,4=Vx,1+Vx,2+Vx,3+Vx,4 \tag{85}$$

Because of the leakage inductance are same, so Vz,1=Vz,2=Vz3=Vz,4=Vz, then

$$V_Z = \frac{Vx,1 + Vx,2 + Vx,3 + Vx,4}{4} \tag{86}$$

For D<0.25, when any switch is on, one of Vx nodes becomes Vin, others are equal to zero. Therefore,

$$V_Z = \frac{Vin}{4} \tag{87}$$

The voltage waveform of the key nodes of the circuit is shown in Fig.41.

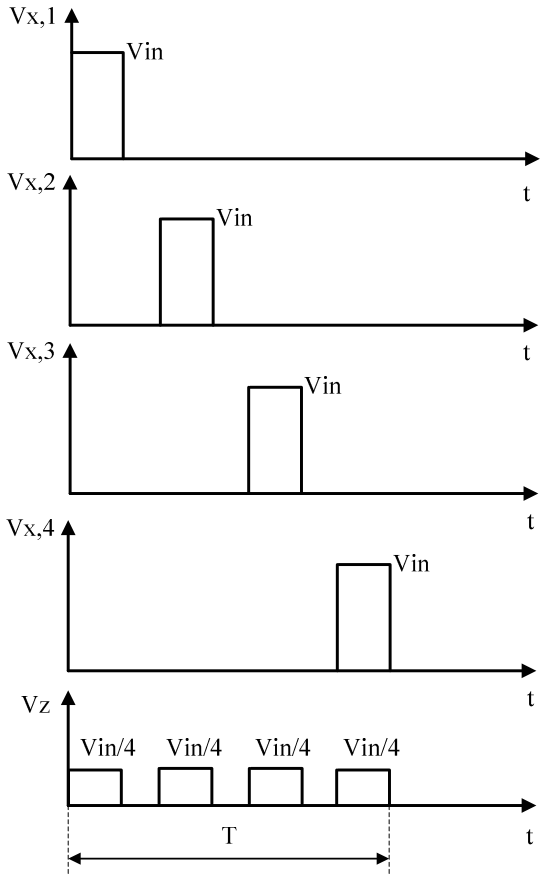

Fig. 41. Nodes voltage waveforms.

For the leakage inductances, this is like having a converter running from an equivalent input voltage Vin,eq=Vin/4, switching at four times the actual switching

frequency f. The on-time is unchanged, but the apparent duty cycle is four times the original duty cycle, so that the output voltage is the same as without coupling.

The phase current ripple and capacitor current ripple of proposed structure can be derived as

$$\Delta Iphase,coup = \frac{(Vz - Vo)DT}{2Lk} = \frac{(\frac{1}{4} - D)VinDT}{2Lk}$$
$$\Delta Ic,coup = 4\Delta Iphase = \frac{(1-4D)VinDT}{2Lk} \tag{88}$$

To make a fair comparison with the uncoupled case, we consider equal energy storage in nominal dc conditions, which implies that the values of the leakage inductances are equal to the values of the uncoupled inductors. Therefore, for conventional 4-phase buck with uncoupled inductors, the ripple can be derived as

$$\Delta Iphase,uncoup = \frac{(Vin - Vo)DT}{2Lk} = \frac{(1-D)VinDT}{2Lk}$$
$$\Delta Ic,uncoup = \frac{(1-4D)VinDT}{2Lk} \tag{89}$$

Comparing (88) with (89), the capacitor ripple current is unchanged, due to the fact the energy storage inductance is the same, while the phase current ripple is reduced by proposed structure as

$$\frac{\Delta Iphase,coup}{\Delta Iphase,uncoup} = \frac{\frac{1}{4} - D}{1-D} \tag{90}$$

Fig.42 shows the phase current ripple reduction with proposed structure at different operating points.

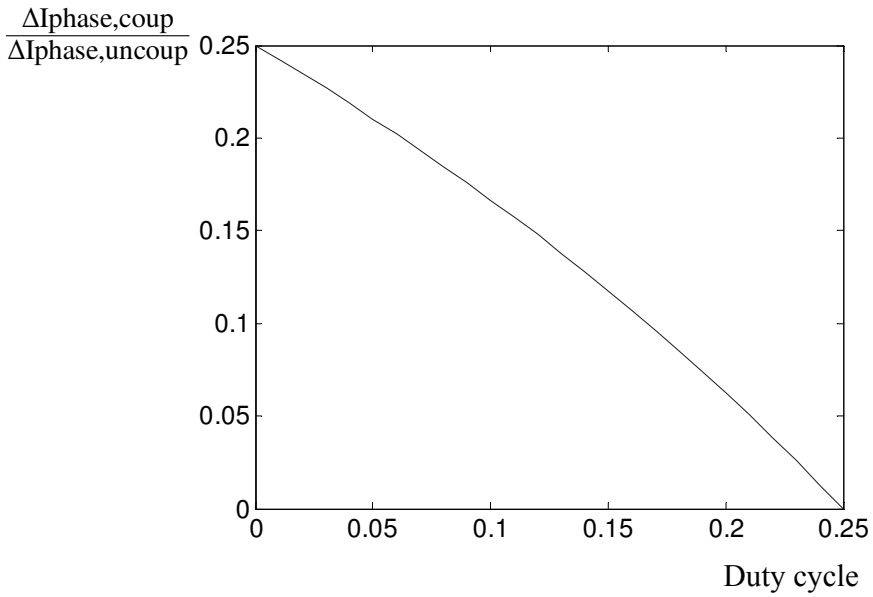

Fig. 42. Phase current reduction.

It can be seen from the figure that increasing the duty cycle can further reduce the phase current ripple. And D=0.25 is the zero phase current ripple case.

The above analysis is only done on a 4-phase interleaved buck converter with proposed structure. However, the proposed structure can be extended to other phase numbers. The derivation is similar therefore not done here. For N-phase buck converter with proposed structure, the phase current ripple reduction can be proved to be

$$\frac{\Delta Iphase,coup}{\Delta Iphase,uncoup} = \frac{\frac{1}{N} - D}{1 - D} \tag{91}$$

Fig.43 shows an alternative structure to proposed structure, and the analysis is similar. It can be proved the coupled inductor at the output forces the phase current I11 and I22 to be equal. The coupled inductor supplying I11 forces its two branches I1 and I2 to be

equal. Similarly the one providing I22 also makes its phase current I3 and I4 to be the same.

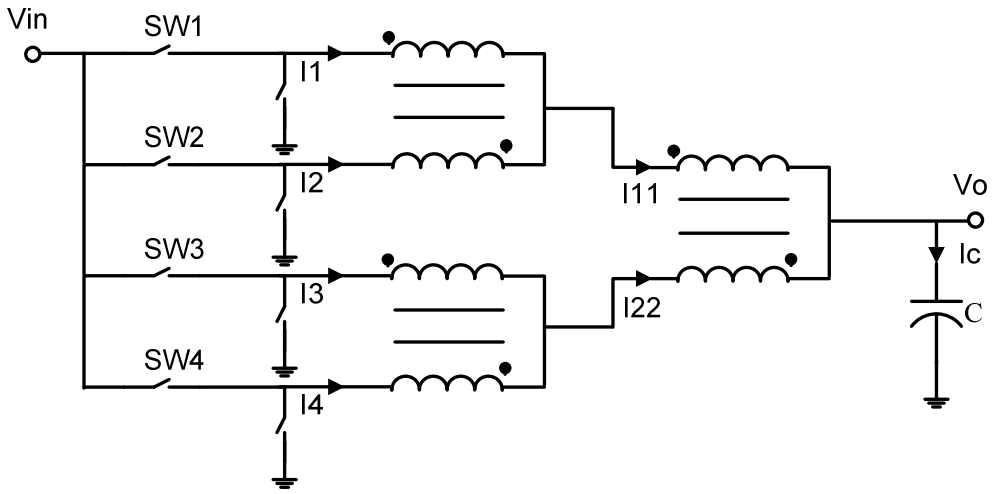

Fig. 43. Alternative structure.

4.2 Proposed new structure with parasitic components

Fig.44 shows a practical model with parasitic components, which include switch on resistance Rds,on, diode voltage drop Vd and leakage inductance resistance DCR.

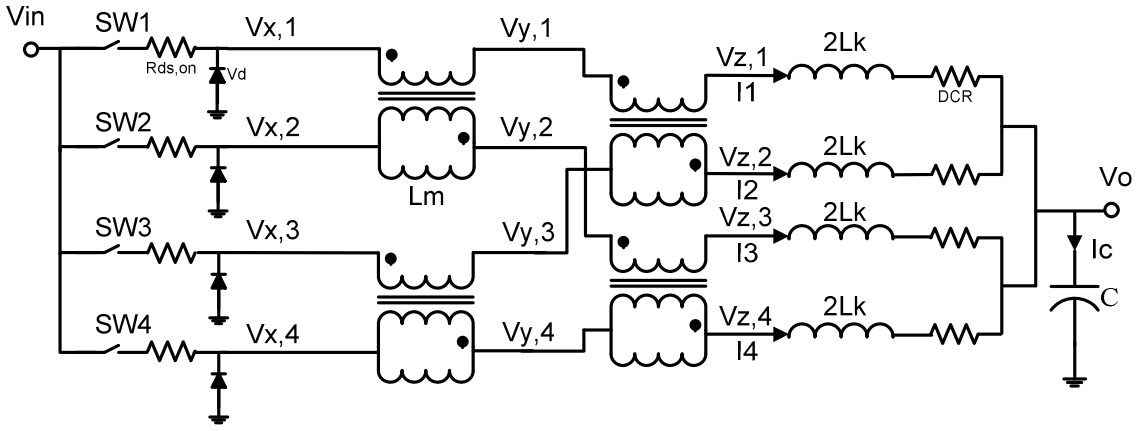

Fig. 44. Proposed structure with parasitic components.

It is well known for buck converter including these parasitic components has the voltage transfer ratio as

$$Vo = (Vin - V_{DS}) \times D - V_d \times (1 - D) - I_L \times DCR \tag{92}$$

When SW1 is on, Vx,1 is equal to Vin minus the voltage drop due to on resistance. At the same time, other switches are off, hence Vx,2, Vx,3, Vx,4 is equal to negative the diode voltage drop. Fig.45 shows the voltage waveforms of the nodes.

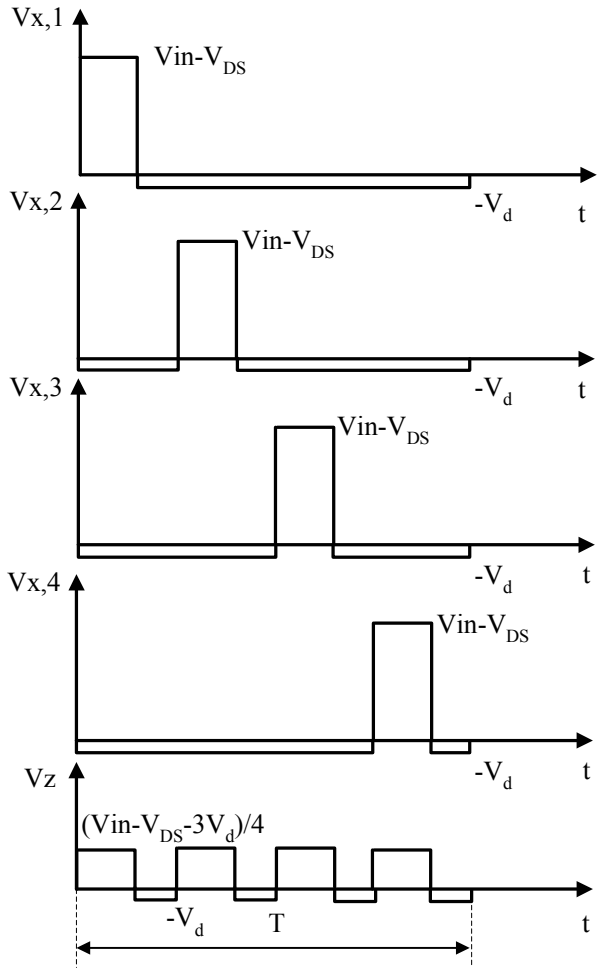

Fig. 45. Nodes voltage waveforms.

As the leakage inductance and the voltage drop over DCR is same, positive Vz and negative Vz can be found as

$$\begin{aligned} Vz+ &= \frac{Vin - V_{DS} - 3V_d}{4} \\ Vz- &= -V_d \end{aligned} \tag{93}$$

Then the phase current ripple and capacitor current ripple will become

$$\begin{aligned} \Delta Iphase, coup &= \frac{(Vz - Vo - V_{DCR})DT}{2Lk} \\ \Delta Ic, coup &= 4\Delta Iphase = \frac{2(Vz - Vo - V_{DCR})DT}{Lk} \end{aligned} \tag{94}$$

where V_{DCR} is the voltage drop over leakage inductance DCR.

4.3 Design example

A 4-phase buck converter is designed with input voltage 12V, output voltage 1.5V and power 150W. Based on the parameters, duty cycle can be found as

$$D = \frac{Vo}{Vin} = 0.125 \tag{95}$$

According to power and output voltage, the load resistance can be calculated as

$$R = \frac{Vo^2}{P} = 0.015\Omega \tag{96}$$

As the total output current is 100A, the DC current of each phase is 25A. With a peak-to-peak phase current ripple limit of 1%, which is 0.25A, based on (88), the leakage inductance of the coupled inductor can be found as

$$Lk = \frac{(\frac{1}{4} - D)VinDT}{2\Delta Iphase} = 1875nH \tag{97}$$

For uncoupling case with the individual inductance equal to the leakage inductance, the phase ripple current is

$$\Delta Iphase = \frac{(Vin - Vo)DT}{2Lk} = 1.75A \tag{98}$$

Therefore, the phase current ripple is reduced by about 85%.

4.4 Simulation results

Fig.46 shows the simulated waveforms based on the design parameters. The phase current peak-to-peak ripple is measured to be 0.25A, meeting the 1% ripple requirement. And the capacitor current ripple is 1A, which is exactly four times the phase current ripple, due to the fact all four phase currents are exactly the same and overlap each other. In addition, both the phase current and capacitor current ripple frequency is increased to 4 times the switching frequency, as in every switching cycle, four switches will be turned on and off.

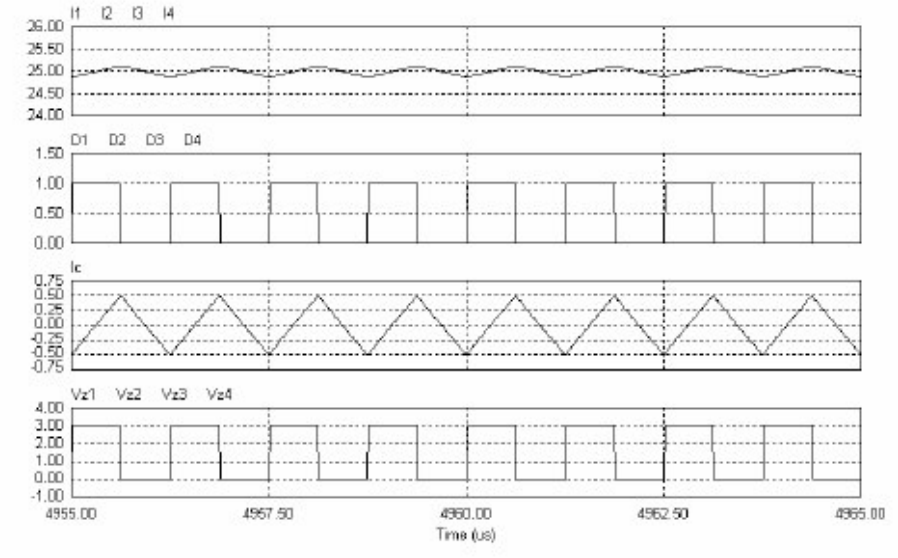

Fig. 46. Simulated waveforms of proposed structure.

Compared to Fig.46 for coupled inductors, Fig.47 shows the waveforms of conventional four-phase buck converter with uncoupled inductors. As the individual inductance is set equal to the leakage inductance in the coupled inductor, the capacitor current ripple is the same and the ripple frequency is four times the switching frequency. However, the phase current is still at switching frequency, and the peak-to-peak ripple is 5 times that of proposed structure.

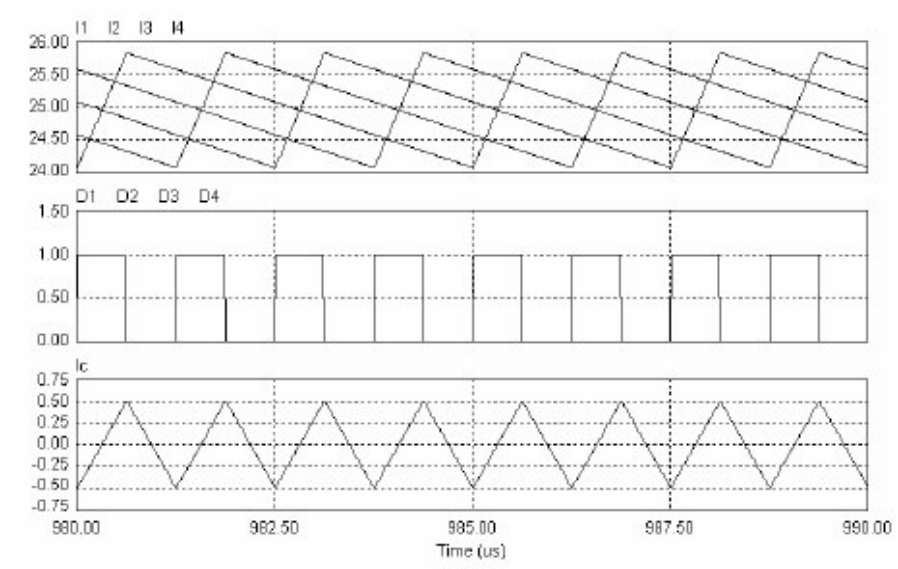

Fig. 47. Simulated waveforms of conventional four-phase buck converter.

Fig.48 shows the waveforms of proposed structure with input voltage changed to 6V and hence the duty cycle becomes 0.25. According to (88), both the phase current ripple and capacitor current ripple becomes zero, indication D=0.25 is the best operating point for 4 phase buck converter with proposed structure. On the other hand, for conventional 4 phase buck converter, D=0.25 is the zero output current ripple point, but the phase current ripple still exists.

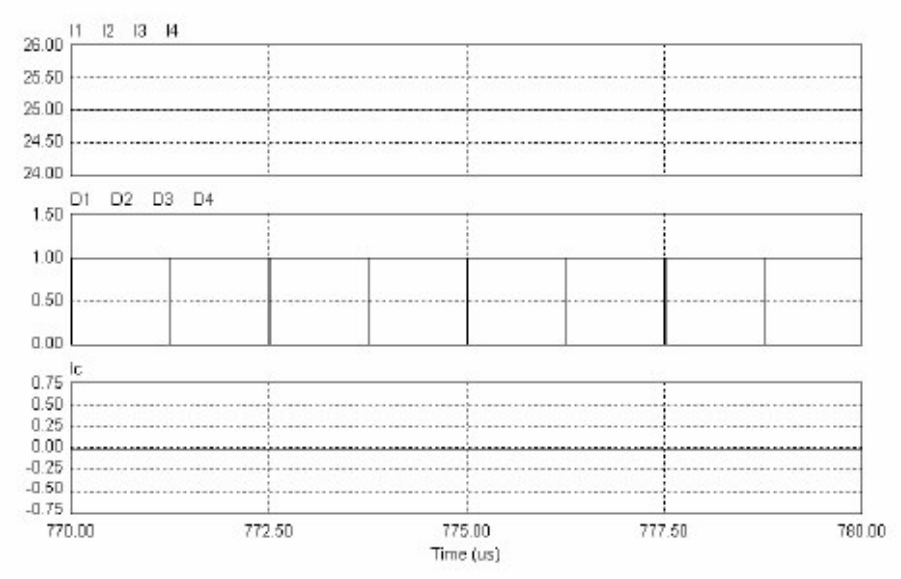

Fig. 48. Zero current ripple case.

4.5 Conclusions

This chapter proposes a new structure for multiphase DC-DC converter using coupled inductors. It has been shown with proposed structure the multiphase buck converter has excellent current sharing characteristic, reduced current control complexity, reduced phase current ripple and increased phase current ripple frequency.

CHAPTER V
CONCLUSIONS

5.1 Summary

In this thesis, multiphase DC-DC converter with directly coupled inductors and inversely coupled inductors are discussed and analyzed. First, directly coupled inductors are applied to multiphase interleaved boost converter to achieve overall input current reduction. Equivalent inductances in different modes have been derived. In addition, mathematical derivation has been done on the phase current ripple and overall input current ripple. This concept has been finally validated by both simulation and experiments. Secondly, multiphase DC-DC converters with inversely coupled inductors has been discussed and analyzed. It is found by carefully choosing appropriate operating points and coupling coefficient, the phase current ripple and overall current ripple can be effectively reduced. Thirdly, a new structure using coupled inductors is proposed for multiphase DC-DC converters. It is analyzed and validated by computer simulation to have the benefits of excellent current sharing performance, reduced current control complexity and reduced phase current ripple.

5.2 Future work

Future research of applying coupled inductors to multiphase DC-DC converters will involve extending the concepts to other types of multiphase DC-DC converters. For example, the concept of overall input current ripple reduction of multiphase boost converter based on directly coupled inductors, which is proposed in chapter II, can be extended to multiphase buck converter, in order to achieve output current ripple reduction,

which may have the benefit of lowering the output capacitance requirements. The analysis will be similar. Further, as mentioned in chapter III, by carefully choosing the coupling coefficient, phase current ripple reduction of multiphase boost converters with inversely coupled inductors can be achieved. In addition, in chapter IV, the proposed new structure is validated by computer simulations. Therefore, future work involves hardware demonstration of this concept.

REFERENCES

[1] D.J. Perreault, and J.G. Kassakian, "Distributed interleaving of paralleled power converters," *IEEE Trans. Circuits Syst. I Fundamental Theory Appl.*, vol.44, pp. 728-733, 1997.

[2] M. S. Elmore, "Input current ripple cancellation in synchronized, parallel connected critically continuous boost converters," in *Proc. IEEE APEC'96*, Mar 1996, vol.1, pp.152-158.

[3] C. Chang, and M.A. Knights, "Interleaving technique in distributed power conversion systems," *IEEE Trans. Circuits Syst. -I: Fund. Theory Appl*., vol.42, no.5, pp. 245 – 251, 1993.

[4] D.K. W. Cheng, X. C. Liu, and Y.S. Lee, " A new modified boost converter with ripple free input current by using coupled inductors," in *Proc. IEE Int. Conf. Power Electronics and Variable Speed Drives*, London, U.K., Sep 1998, pp.592-599.

[5] M.T. Zang, M.M. Jovanovic, and F.C. Lee, "Analysis and evaluation of interleaving techniques in forward converters," *IEEE Trans. Power Electron.*, vol.13, no.4, pp. 690-697, 1998.

[6] B.A. Miwa, D.M. Otten, and M.F. Schlecht, "High-efficiency power factor correction using interleaving techniques," in *Proc. of IEEE APEC ' 92*, Feb 1992, vol. 1, pp. 557 – 568.

[7] L. Balogh and R. Redl, "Power-factor correction with interleaved boost converters in continuous-inductor-current mode," in *Proc. IEEE APEC'93*, San Diego, CA, Mar 1993, pp. 168–174.

[8] J.S. Lai and D. Chen, ”Design consideration for power factor correction boost converter operating at the boundary of continuous conduction mode and discontinuous conduction mode,” in *Proc. IEEE APEC'93*, San Diego, CA, Mar 1993, pp.267-273.

[9] J. Wang, W.G. Dunford, and K.Mauch, “A comparison of modified boost converters with continuous inductor current mode and ripple free input current with conventional converters,” in *Conf. Rec. IEEE-IAS Annual Meeting*, San Diego, CA, Oct.1996, vol.2, pp.878-885.

[10] P.A. Dahono, S. Riyadi, A. Mudawari, and Y. Haroen, “Output ripple analysis of multiphase DC – DC converter,” in *Proc. of IEEE Intl Conf. on Power Electronics and Drive Systems PEDS*, Jul 1999, pp. 626 – 631.

[11] R. Giral, L. Martinez, J. Calvente, R. Leyva, and E. Vidal, “Self-oscillating interleaved boost regulator with loss free resistor characteristic,” in *Proc. of ISCAS' 97*, Jun 1997, pp. 825 – 828.

[12] R. Giral., L.M. Salamero, R. Leyva, and J. Maixe, “Sliding-mode control of interleaved boost converters,” *IEEE Trans. Circuits Syst.*, vol.47, no.9, pp. 1330-1339, 2000.

[13] M. Veerachary, “Analysis of interleaved dual boost converter with integrated magnetics: signal flow graph approach,” *IEE Proc. Electr. Power Appl.*, vol.150, no.4, pp. 407 – 416, 2003.

[14] W. Wen, and Y. Lee, “A two-channel interleaved boost converter with reduced core loss and copper loss,” in *Proc. of IEEE PESC' 04*, Jun 2004, vol. 2, pp. 1003 – 1009.

[15] J. W. Kolar, G. R. Kamath, N. Mohan, and F. C. Zach, "Self-adjusting input current ripple cancellation of coupled parallel connected hysteresis - controlled boost power factor correctors," in *Proc. IEEE Power Electron. Spec. Conf.*, Jun 1995, pp. 164–173.

[16] Q. Zhao and F. C. Lee, "High-efficiency, high step-up dc–dc converters," *IEEE Trans. Power Electron*., vol. 18, no. 1, pp. 65–73, Jan 2003.

[17] P. Wong, F. C. Lee, X. Jia and D. van Wyk, "A novel modeling concept for multi-coupling core structures," in *Proc. IEEE APEC*, Mar 2001, pp.102-108.

[18] R. Prieto, J. A. Cobos, O. Garcia and J. Uceda, "Interleaving techniques in magnetic components," in *Proc. IEEE APEC*, Feb 1997, pp. 931-936.

[19] P. Zumel, O. Garcia, J.A. Cobos, J. Uceda, "Magnetic integration for interleaved converters", in *Proceedings of APEC 2003*., Feb 2003, pp. 1143–1149.

[20] *LabVIEW FPGA Module User Manual*, Austin, TX: National Instruments, Mar. 2004.

[21] R.W. Erickson, and D. Maksimovic, *Fundamentals of Power Electr*onics, 2nd ed., Boston, MA: Kluwer Academic, 2001.

[22] N. Mohan, T. M. Undeland, and W. P. Robbins, *Power Electronics: Converters, Applications, and Design*, New York: Wiley, 1995.

[23] T.W. Martin and S.S. Ang, "Digital control of switching converters," *IEEE Symposium on Industrial Electronics*, vol. 2, pp. 480-484, 1995.

[24] A. Prodic, D. Maksimovic, "Digital PWM controller and current estimator for a low-power switching converter," in *Proc. of the 7th IEEE Workshop on Computers in Power Electronics,* July 2000, pp.123-129.

[25] S. Choudhury, *Designing a TMS320F280x Based Digitally Controlled DC - DC Switching Power Supply*, Dallas: Texas Instruments, 2005.

VITA

Meng Shi was born in Shanghai, China in 1982. He received his Bachelor of Engineering degree from School of Electrical & Electronics Engineering, Shanghai Jiao Tong University, Shanghai, China in 2004.

He joined the master's program in Electrical Engineering at Texas A&M University, College Station in 2005, and received his Master of Science degree in 2007. His research interests include DC-DC converter design and magnetic design.

He can be reached through Dr. Prasad Enjeti of Department of Electrical Engineering, Texas A&M University, College Station, TX 77843-3128.